國 立 交 通 大 學

電信工程研究所

碩 士 論 文

設計加入集總式元件的微小化蕈狀式結構並使用此蕈狀式結構來加強小天線的輻射效率

Design of Compact Mushroom Structure with Lumped Elements to Improve the Performance of Small Antennas

研究生： 蔡博丞 (Po-Cheng Tsai)

指導教授：黃謀勤 博士 (Dr. Malcolm Ng Mou Kehn)

中 華 民 國 102 年 8 月 30 日

設計加入集總式元件的微小化蕈狀式結構並使用此蕈狀式結構來加強小天線的輻射效率

Design of Compact Mushroom Structure with Lumped Elements to Improve the Performance of Small Antennas

研 究 生：蔡博丞　　Student：Po-Cheng Tsai

指導教授：黃謀勤　　Advisor：Malcolm Ng Mou Kehn

國 立 交 通 大 學

電信工程研究所

碩 士 論 文

A Thesis

Submitted to Institute of Computer and Information Science

College of Electrical Engineering and Computer Science

National Chiao Tung University

in partial Fulfillment of the Requirements

for the Degree of Master

in

Communication Engineering

August 2013

Hsinchu, Taiwan, Republic of China

中華民國一〇二年八月

設計加入集總式元件的微小化蕈狀式結構並使用此蕈狀式結構來加強小天線的輻射效率

學生：蔡博丞　　指導教授：黃謀勤　博士

國立交通大學電信工程研究所碩士班

摘　　要

在此論文中，我們希望以一個簡單且明瞭的方式來設計出微小化的蕈狀結構，因此我們將利用集總是元件來達成製作微小化蕈狀結構，而不是利用複雜的電路方式例如指叉式電容和狀蛇行線。 此微小化的蕈狀結構設計主要是利用集總式元件使其本身的電磁間隙能夠往低頻移動，我們可以利用傳輸線的觀念來解釋當一系統本身加入更多的電容電感的效應後，其操作頻率會受到電容電感的影響而產生在較低頻的範圍，進而達成微小化的目標。 在本論文中，我們將以三種方式來分析微小化蕈狀結構，第一種是利用色散圖來分析，此方法的優點是他是一個完整的分析模型可以準確的判斷出電磁間隙的所在頻段，第二種是利用散射參數來分析，此方法是能夠以實驗方式來觀察電磁間隙，第三種則是改良式的等效電路模型，他將會以比前兩種方法都還要快的速度來分析此微小化蕈狀結構。此外我們還會再設計出兩種天線：貼片天線以及複合式左右手微小化天線，其操作頻率均會在微小化蕈狀結構的電磁間隙中，用來印證此微小化蕈狀結構能夠使天線輻射效率加以提升。

Design of Compact Mushroom Structure with Lumped Elements to Improve the Performance of Small Antennas

student：Po-Cheng Tsai Advisors：Dr. Malcolm Ng Mou Kehn

Institute of Communications Engineering
National Chiao Tung University

ABSTRACT

In Thesis, the new type of compact mushroom structure had been proposed. The original equivalent circuit transmission line model tells that the electromagnetic bandgap (EBG) range can be affected by its equivalent capacitor and inductor. So this thesis propose the simple way to shift down the EBG range by inserting lunped element, instead of complex design, such as interdigital capacitor and meander line. Also we use three methods to analyze the compact mushroom structure, dispersion diagram, S-parameters measurement, and modified equivalent circuit model. Three of them have different advantage for analyzing. Dispersion diagram provides the complete analysis for compact mushroom structures, S-parameter measurement is the only way to observe the effects of EBG practically, and modified equivalent circuit model have the quicker way to find out the bandgap range. In addition, patch antenna and CRLH small antenna are designed to combine with compact mushroom structure, to prove that the radiation efficiency of both antenna can be improved by compact mushroom structure.

誌　　謝

首先最先要感謝的就是我的指導教授：黃謀勤博士，他總是不厭其煩的指導我如何培養專業的研究態度，以及在專業上的指導，並且在碩士生涯這漫漫長路上給予我一個正確的方向，讓我在電磁領域上能夠窺知一二。

再來，要特別謝謝我實驗室的兩位同學，建融和怡嘉，在這兩年我們一起分擔實驗室的大小事，不管是學業上互相討論交流，或是私底下相約吃大餐，因為有他們所以能夠在 923 實驗室過得非常快樂。儘管兩年來的路途遙遙，口試前的煎熬時光也因為有他們所以才能順利度過。同時也謝謝實驗室的學弟們：南更、宗聖、偉全以及永勳，他們的加入讓實驗室更加歡樂，讓實驗室的生活更多采多姿。還有要特別感謝的是已經畢業的學長：大龍及樞彥，他們儘管已經畢業了，還是隨時的給予我們經驗上的指導，然後也要謝謝其他實驗的博班學長：宜哲，不管是在論文上面的研究或是技術上的交流，他總是不遺餘力的糾正我研究上的錯誤及給予適當的指導，也謝謝在電波組的同學；奕心、學群、宏偉、則宇等，也謝謝他們不管是在找工作或是口試前的準備，我們總是互相鼓勵，謝謝他們平時的幫忙。也謝謝其他實驗室的學弟：錦政，謝謝他幫忙我製作研究上的實作。

最後要謝謝我的家人，讓我能夠在安穩的環境下，全心全意的投入碩士的研究，也謝謝我的女朋友，在我最感疲憊的時候給予精神上的支持，謝謝你們無條件的支持與付出，我才能夠順利的完成學業。

TABLE OF CONTENTS

LIST OF FIUGURES

LIST OF TABLES

Chapter 1 Introduction

A new type of electromagnetic structure commonly referred to as the mushroom surface had been developed in 1999, lending itself to new methods to improve the performance of antennas. As long as the inserted structures, called cells, are very small compared to the propagating wavelength, they can create a macroscopic effect on the electromagnetic wave as they pass through the new medium [1]. Those effects can be called high impedance surface (HIS) or electromagnetic bandgap (EBG) properties. While a conductive surface is a good reflector, it has the unfortunate property of reversing the phase of the reflected wave [2]. The flat metal sheet produces the reverse phase shift when the distance gets smaller than $\lambda/4$ between antenna and ground, and it will reflect the destructive interference wave to reduce the radiation wave by the antenna. The HIS is the method to solve this problem in antenna design. Another property of the structure is that it can produce an electromagnetic bandgap over a certain frequency range. It means that no surface waves can propagate in this band. Over the years of antenna developments, the patch antenna has become an important application in antenna engineering. Inevitably, the patch antenna always excites the surface wave propagating between the air and substrate; it will become a multipath interference that reduces the performance. The EBG structure is the way to solve this problem, as long as the resonant frequency operates within the bandgap, the surface wave will be suppressed. In recent years, antenna developments are focused on miniaturization, such as using meander lines, interdigital capacitors, shorting pins, and lumped elements etc. But the antenna size and its performance are strongly linked together [3]. So we take advantage of the EBG structure to improve the antenna's

performance [4] and [5]. In the meantime, the ground plane size comprising the EBG structure is usually ignored. But the size of the EBG structure is larger than the small antenna. The antenna, including the ground plane, is thus no longer miniaturized.

For those reasons, we focus on how to reduce the electrical size of the EBG structure to realize the *truly* compact, small, but yet still good-performing antenna with EBG structure, without the facade of a large ground plane excluded from the total size. The size of the EBG structure is dependent on the frequency range of the bandgap, so if the bandgap can be shifted down to lower frequencies in the spectrum, we will have a compact EBG structure. In this thesis, we propose an idea of utilizing lumped elements to shift down the frequency band of the EBG structure, and we can use this compact ground plane to combine with the small antenna, improving the performance, such as the radiation efficiency and gain.

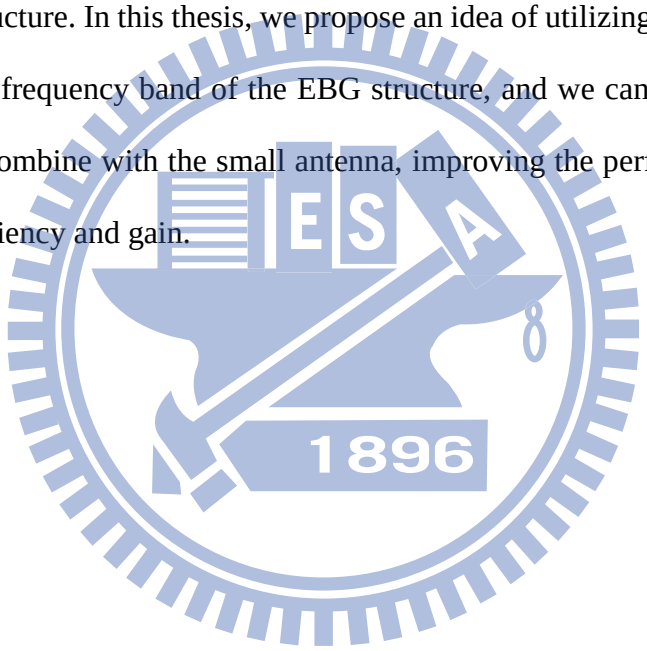

Chapter 2 Mushroom structure

2.1 Introduction

In recent years, there has been growing interest in utilizing electromagnetic EBG structure in the electromagnetic and antenna community [6], and a lot of different types of EBG structures have been developed for reducing the size of the EBG structure [5] [6]. In this thesis, we choose the mushroom structure as the research body of which the operation frequency range of the EBG is to be modified; reduced to be specific. The mushroom structure, a kind of EBG structure, shown in Figure 2.1, is a periodic structure characterized by a substrate filled with an array of vertical metallic via posts, each capped by a capacitive frequency selective surface [7]. The advantages of the mushroom structure include ease of fabrication into any substrates, and convenient but accurate determination of the operating EBG by equivalent transmission line models. Recently, the mushroom structure was developed for reducing the operating EBG by modifying the shape of the mushroom structure, such as adding interdigital capacitors and spirals to increase the capacitance and inductance respectively [8]-[10]. Here, we propose a new method to find the analytic TM wave solution, so as to predict the TM wave and compare with the dispersion diagram generated by HFSS simulation. In reality, we cannot get the dispersion diagram of actual fabricated structures by practical measurements. Nonetheless, implicit information about the surface-wave passbands and bandgaps may be acquired through the scattering-parameters (S-parameters). In S-parameter measurements, we can find the frequency bandgap from the S21 parameters. However, we can only find the TM wave at one time, as the TE wave will be forbidden from being manifested by the S-parameters. So we cannot decide the position of frequency bandgap from the S-parameter diagram (specifically, the graph of

S21 vs. frequency). The main point of using the S-parameter diagram is for its comparison with the dispersion diagram generated theoretically (by simulations); if the frequency bandgap indicated by the dispersion diagram is the same as that implied by the S-parameter diagram, then we can be sure about the validity of that frequency bandgap. Because the mushroom structure can be represented by a transmission line circuit model, there is motivation to combine lumped elements with the mushroom structure. The mushroom structure with lumped elements may then be analyzed by the equivalent circuit. In the following section, we will introduce the transmission line circuit model of the mushroom structure, from which the analytic TM wave solution of the mushroom structure may be obtained. Otherwise the HFSS and CST full-wave simulation software solvers will be used, respectively to determine the bandgaps of the mushroom structure through the dispersion diagrams that they are able to generate and to compute the S-parameter diagram for comparing with practical measurements.

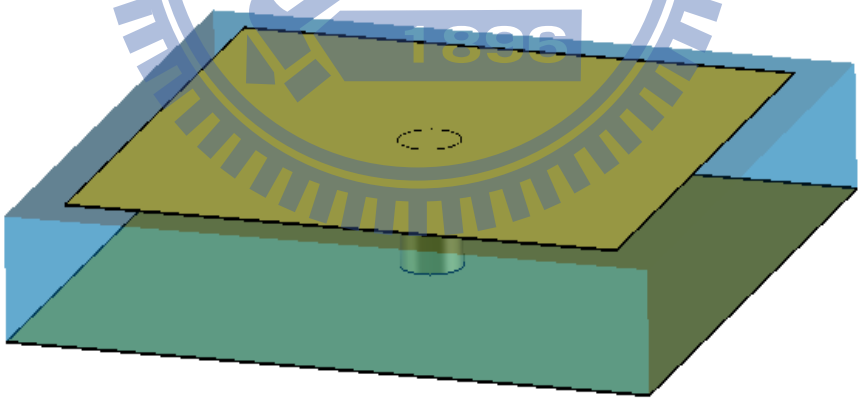

Figure 2.1 Mushroom structure

2.2 Equivalent circuit

After we understand what the mushroom structure is, we have to use a simple way to analyze it. Figure 2.2 shows the cross-sectional view of the mushroom structure, with patch width w, gap size between patches g, substrate thickness h, radius of via r, and

dielectric constant ε_r of the dielectric host. A voltage applied parallel to the surface causes charge buildup on the ends of the plates, which can be described as a capacitance. As the charges slosh back and forth, they flow around a long path through the vias and the bottom plate. Associated with these currents is a magnetic field, and thus an inductance [2]. Summing up the above description, we can represent the pictorial schematic of Figure 2.2 by the equivalent circuit model of Figure 2.3.

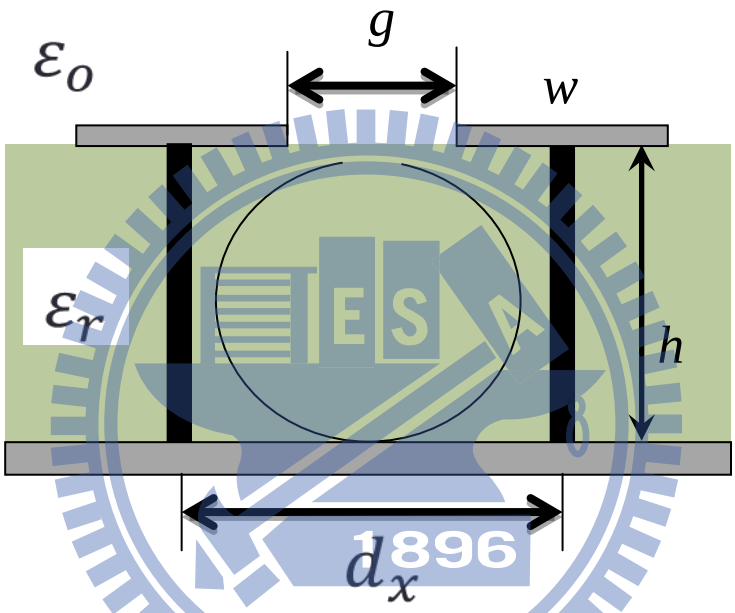

Figure 2.2 The cross section view of mushroom structure

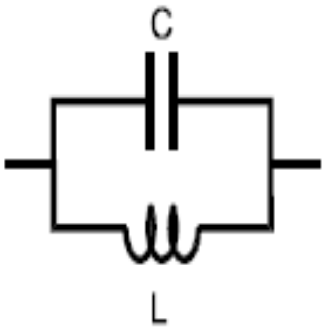

Figure 2.3 The equivalent circuit of mushroom structure

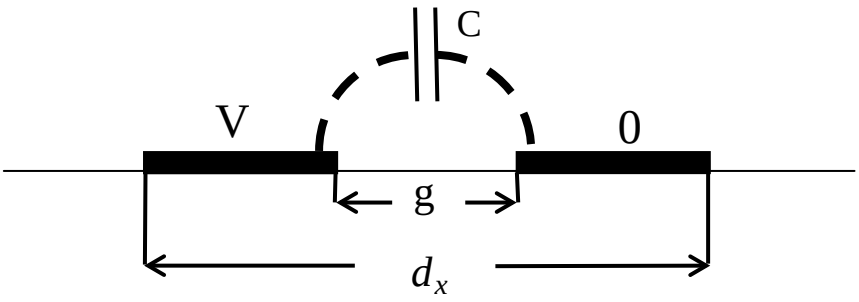

Figure 2.4 The conformal mapping of fringing capacitance

Even Figure 2.3 is still just a brief diagram, although it does provide the main idea for understanding how the mushroom structure works. More detailed derivation will be given below. We know that the adjacent metal patches give rise to fringing capacitance, the representation of which can be derived using conformal mapping, a common technique for solving two dimensional electrostatic field distributions, as shown in Figure 2.4. By conformal mapping, the electric flux function for this geometry is described by the following equation [2]. First we should use the flux function for this geometry by Eq.(1.1), and then assume that $g << d_x$ Eq. (1.1) is subsequently approximated to Eq. (1.2).

$$\psi = \mathrm{Im}[\frac{\varepsilon V}{\pi}\cos^{-1}\left(\frac{x+jy}{g/2}\right)] \tag{1.1}$$

$$\psi \approx \mathrm{Im}[\frac{2\varepsilon V}{\pi}\cos^{-1}(\frac{a}{g})] = \frac{2\varepsilon V}{\pi}\cosh^{-1}(\frac{d_x}{g}) \tag{1.2}$$

The flux ending on one plate is equal to the charge on that plate, which is equal to the product of the capacitance and the voltage across the plate. The edge capacitance between the two plates, called C-fringing, is therefore given by the following expression Eq.(1.3) [2]

$$C_{fringing} = \frac{w(\varepsilon_1 + \varepsilon_2)}{\pi} \cosh^{-1}(\frac{d_x}{g}) \tag{1.3}$$

where *w* is the width of mushroom structure, the metal plate is surrounded by ε_1 and ε_2, and *dx* is the unit cell length of mushroom structure equal to *w* + *g*. The other equivalent capacitance is defined by the parallel capacitance. Assuming the height of the mushroom structure is h, and the permittivity between the two metal plates are ε_r, the parallel capacitance can be acquired by Eq.(1.4) as:

$$C_{parallel} = \varepsilon_r \frac{w^2}{h} \tag{1.4}$$

After every equivalent capacitor of mushroom structure is obtained, we have to determine the total capacitance of the equivalent capacitance. Eq. (1.3) provides the fringing capacitance between adjacent patches, but in this case, Eq .(1.3) is described by one side patch with voltage mapping to the other side patch without voltage. So, by assuming the condition is reversed, we can derive the other fringing capacitance across the same gap. In this condition, the two capacitors can be regarded as parallel. As such, the total capacitance between adjacent patches will be twice the original fringing capacitance. Shown by Figure 2.2, the parallel plate capacitor and fringing capacitor are in series. Hence, we can get the total capacitance of the equivalent circuit of mushroom structure, given by Eq. (1.5).

$$\frac{1}{C_{total}} = \frac{1}{C_{parallel}} + \frac{1}{2C_{fringing}} \tag{1.5}$$

The inductance of the transmission line can be approximated by supposing a solenoid has a cross section $h \times w$ and length w [2]. In this case, magnetic field *H* is represented by Eq. (1.6).

$$H = \frac{I}{w} \tag{1.6}$$

A stored energy of an inductance equals a stored energy of a magnetic energy. So Eq. (1.7) is obtained.

$$I^2 L = \int (\mu H \cdot H) dv = \mu \int |H|^2 \, dv = \mu \left(\frac{I}{w} \right)^2 \cdot h \cdot w \cdot w \tag{1.7}$$

By Eq.(1.7), we can get the inductance associated with the current through the flat metal plate, shown in Eq. (1.8).

$$L_{sheet} = \mu \cdot h \tag{1.8}$$

Currents also flow through the vertical via between the patch and the ground. The inductance of the via can be derived by [11], given by Eq. (1.9).

$$L_{via} = \frac{\mu_0}{2\pi} [h \cdot \ln(\frac{h + \sqrt{r^2 + h^2}}{r}) + (r - \sqrt{r^2 + h^2})] \tag{1.9}$$

In Figure 2.2, we know that L_{sheet} is in series with L_{via}, so the total inductance of the mushroom structure is shown in Eq. (1.10)

$$L_{total} = L_{sheet} + L_{via} \tag{1.10}$$

With the equivalent circuit of the mushroom structure, the surface wave solution may be derived. First we can find an expression relating *k*, α, and ω [2].

$$k^2 = \mu_0 \varepsilon_0 \omega^2 + \alpha^2 \tag{1.11}$$

Eq. (1.11) shows the relationship relating the wavenumber, material parameters, and the frequency for TM surface waves. Using Eq. (1.11) to combine with the impedance of TM surface waves, we obtain Eq.(1.12) [2].

$$Z_{TM} = \frac{j\alpha}{\omega \varepsilon_0} \tag{1.12}$$

By eliminating α, Eq. (1.13) shows the TM wave function k.

$$k_{TM} = \frac{\omega}{c}\sqrt{1 - \frac{Z^2}{\eta^2}} \tag{1.13}$$

Where the η is the impedance of free space, c is the light speed in vacuum, and Z is the reactance in Figure 2.3, shown in Eq. (1.14).

$$Z = \frac{j\omega L_{total}}{1 - \omega^2 L_{total} C_{total}} \tag{1.14}$$

The TE wave can be also derived in the same way by combining Eq. (1.11) with the following Eq. (1.15).

$$Z_{TE} = \frac{-j\omega \mu_0}{\alpha} \tag{1.15}$$

Then the propagation constant of TE mode is shown in Eq.(1.16)

$$k_{TE} = \frac{\omega}{c}\sqrt{1-\frac{\eta^2}{Z^2}} \tag{1.16}$$

After establishing the concepts of the equivalent circuit of mushroom structure, we will use the modified method to generate the TM and TE modal dispersion diagrams, as given by Figure 2.5. The capacitance and inductance are 0.27pF and 1.13nH respectively.

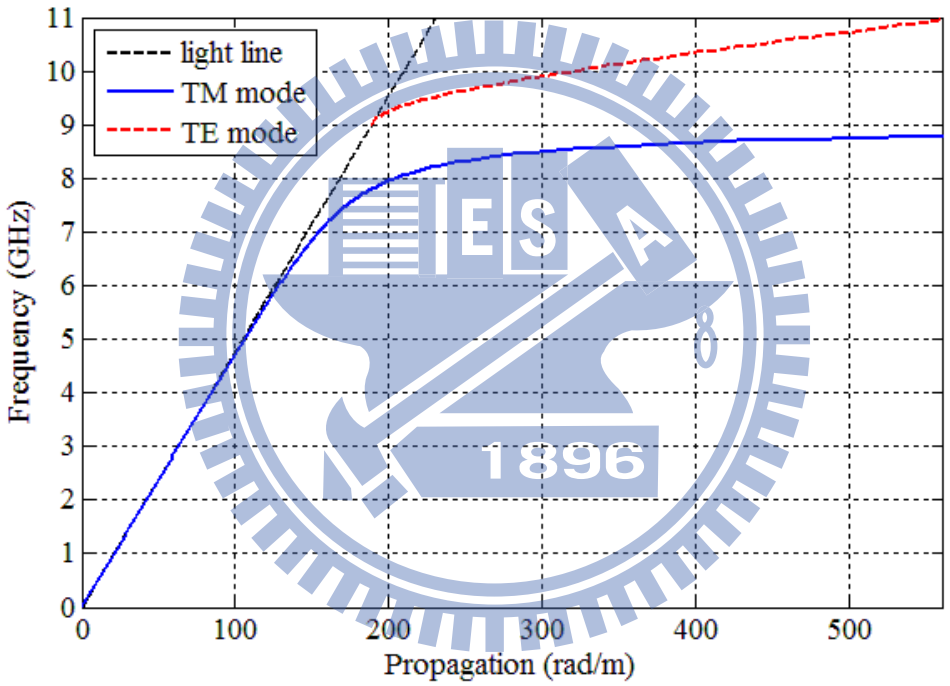

Figure 2.5 TM and TE mode diagram of mushroom structure

2.3 Dispersion diagram

The dispersion diagram constitutes a graph of frequency versus the propagation constant, from which we can know what modes will or will not be excited at a certain frequency. Ordinary structures normally cannot produce electromagnetic band-gaps, so the modal number will rise contiguously with the frequency. But in the EBG structure, the dispersion diagram will produce the band gap as shown in Figure 2.6, and the mode

excitation is not continuous anymore. In Figure 2.5 we can see the red solid-line is for the TM mode, and the blue dashed-line corresponds to a TE mode. These two modes are not continuous, as there is a gap between the solid line and dashed line, constituting the electromagnetic bandgap.

The dispersion diagram is a useful tool to study the electromagnetic band-gap, and we can clearly see that there is no mode excited in the band-gap, which means the wave cannot propagate within the bandgap, and surface waves will be suppressed by the EBG structure at any frequency inside the electromagnetic bandgap.

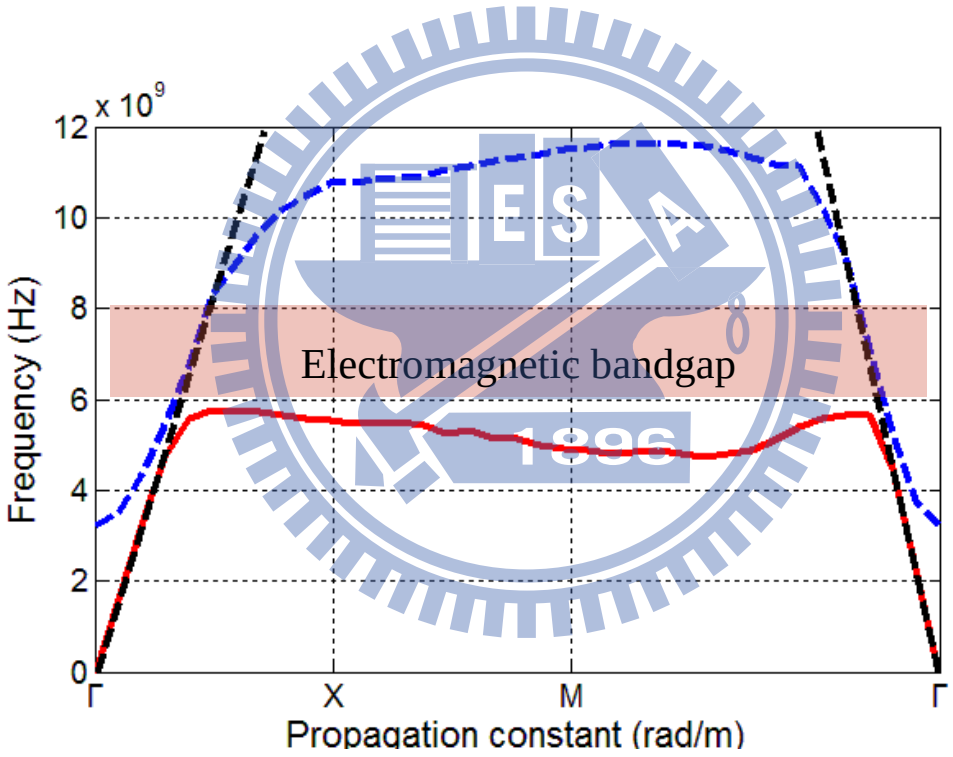

Figure 2.6 Dispersion diagram and electromagnetic bandgap

2.4 **Simulation result and original mushroom structure**

Since we have defined the equivalent circuit of the modified unit cell, we will use simulation software to prove our assumption: that lumped elements can be used to shift down the electromagnetic bandgap. The dimensions of the unit cell are as follow: patch width w = 5mm, cell-size d_x = 5.6mm, substrate thickness h = 0.8mm, radius of via =

0.4mm, and a dielectric slab with relative permittivity of 3.55 is used in this structure. In these dimensions of these initial investigations, we used the HFSS simulation software. Because we want to generate the dispersion diagram, so the boundary must be periodic. At first, we will show the procedure of setting up the simulation for obtaining the dispersion diagram.

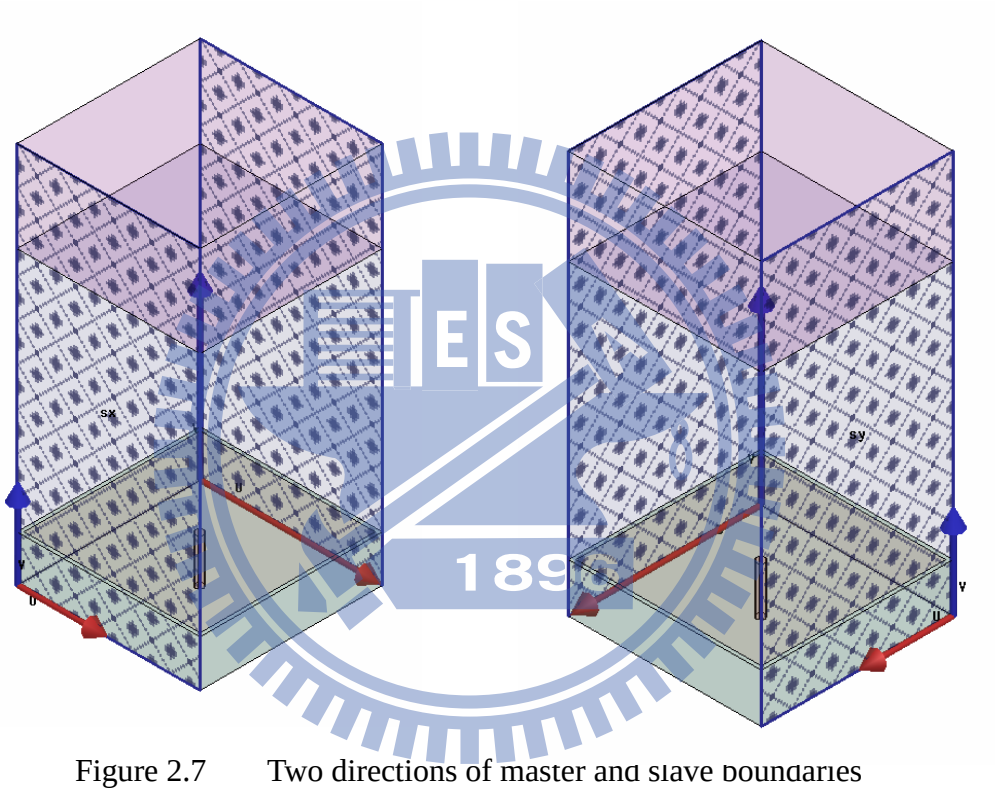

Figure 2.7 Two directions of master and slave boundaries

Figure 2.7 shows the unit cell of the periodic structure, in which the master and slave boundaries are as indicated. Information about master and slaves boundaries may be found as below:

Master and slave boundaries enable to model planes of periodicity where the E-field on one surface matches the E-field on another to within a phase difference. They force the E-field at each point on the slave boundary to match the E-field to within a phase difference at each corresponding point on the master boundary. They are useful for

simulating devices such as infinite arrays

Unlike symmetry boundaries, the E field does not have to be tangential or normal to these boundaries. The only condition is that the fields on the two boundaries must have the same magnitude and direction (or the same magnitude and opposite directions).

Since the dispersion diagram is two dimensional, so in this simulation, we set two master and slave boundaries for two phase shifts. The dispersion diagram includes three parts, and each part has a unique phase shift. In the first part, we set one boundary phase shift from 0 degree to 180 degree, which means only x-direction, and the other master and slave boundaries phase shift is fixed to 0degree, called $\Gamma - X$ part. The second part is call $X - M$ part, in this part one boundary phase shift is fixed to 180 degree, and the other part phase is shifted from 0degree to 180 degree, which means the phase shift is y-direction. The third part is called $M - \Gamma$ part, in this part, one boundary phase shift will be shifted from 0degree to 180 degree at the same time, after that, we just combine these three parts, thereby obtaining the dispersion diagram by simulation software, as shown in Figure 2.8. The first solid line is TM mode and the second dashed is TE mode. The bandgap exists between TM and TE mode, we can see there is no wave propagation in the certain region, about 8GHz to 10GHz.

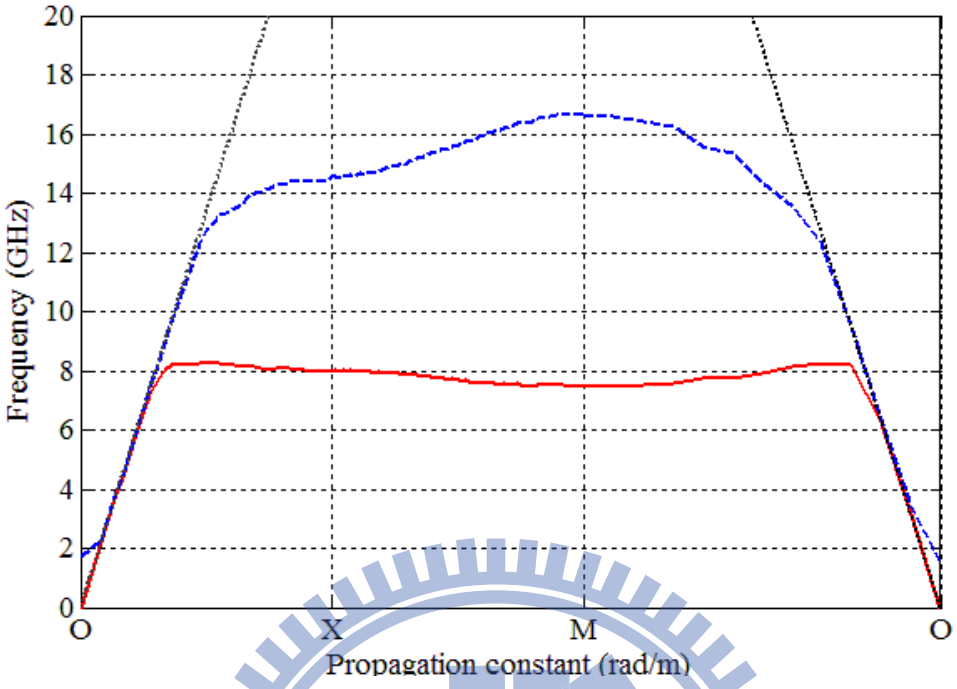

Figure 2.8 Dispersion diagram in HFSS

After obtaining the simulation result of the dispersion diagram, the predictable TM and TE mode diagrams can be compared with HFSS simulation, shown in Figure 2.9. The straight line is the light line, and the three curves are TM mode by different method. The solid curve is produced by HFSS simulation software, the dashed curve is produced by the modified equivalent circuit, and the dotted curve, at the top of three curves by the original unmodified model. By Figure 2.8, we can obtain the conclusion that the modified method is much more agreeing with the HFSS simulation result than the original equivalent circuit method. In the next section, we will propose scattering parameter (S-parameter) simulations by CST simulations to prove the bandgap region, and the advantage of using the S-parameter method is that the theoretical prediction can be observed and validated by actual measurements.

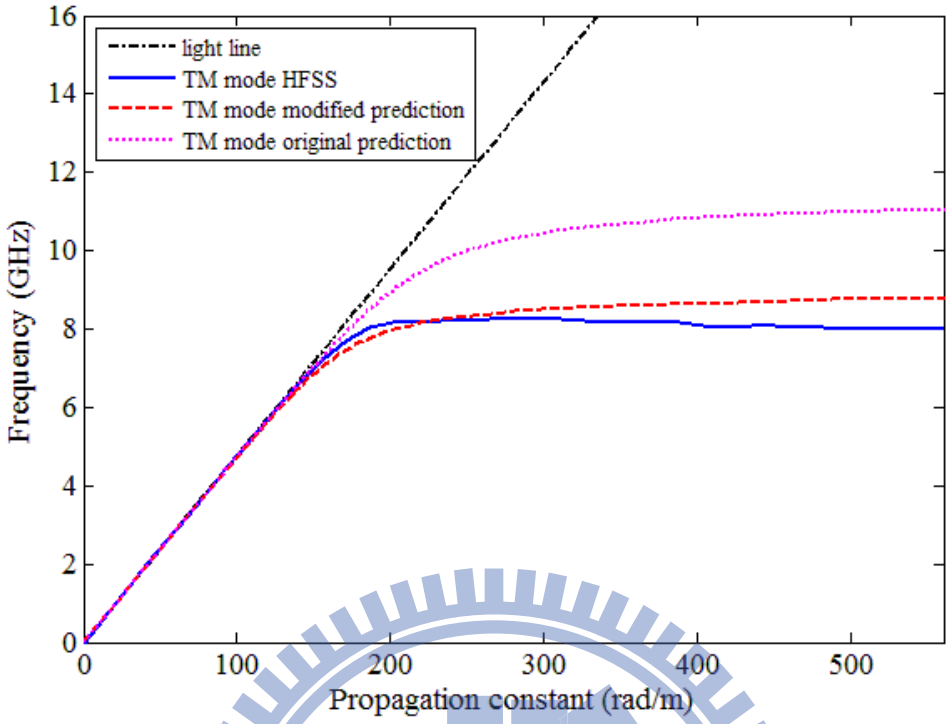

Figure 2.9 The comparison of different predictions of the TM wave

2.5 Scattering parameter simulation and measurement

We have already seen that the dispersion diagram is an effective tool for expressing the size and location of the electromagnetic bandgap. However, we cannot get the dispersion diagram by measurements in reality. So we use the other way to find the bandgap by S-parameter measurement, as was proposed by [2]. We use two coaxial probes as monopole antennas, and connect them to mushroom structure vertically. In that way the TM wave can be excited because the vertical electric field of the probe couples to the vertical electric field of the TM waves, shown in Figure 2.10. The structure consists of two signal coaxial probe, 6×5 patches each with width 5mm and gap 0.6mm, with the radius of via being 0.4mm. The substrate thickness is 0.8mm, and the dielectric constant is 3.55.

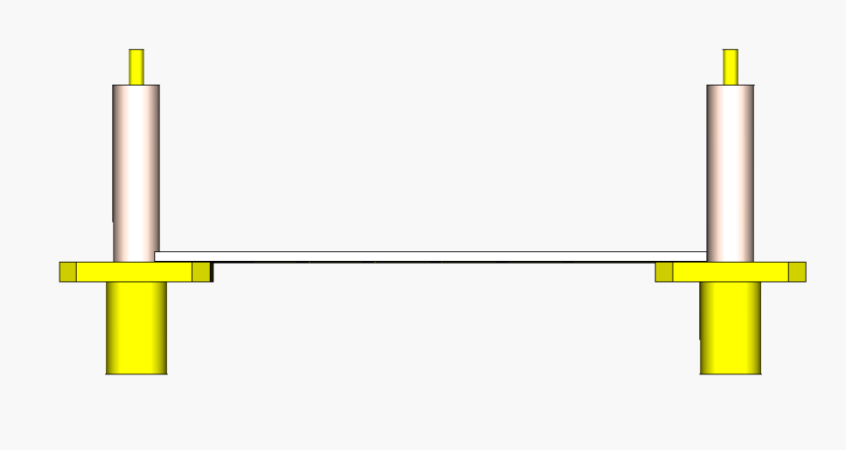

(a)

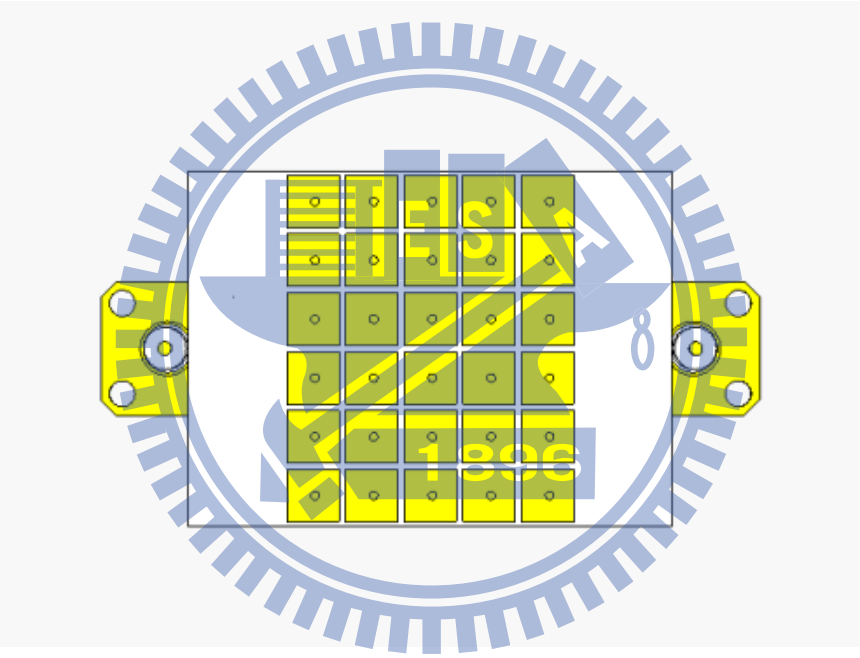

(b)

Figure 2.10 (a) The cross-section view and (b) the top view of S-parameter measurement

The simulation results are shown in Figure 2.11, consisting of two parts, mushroom structure and just the substrate alone. The solid and dashed lines are for the mushroom structure and sole substrate without any copper, respectively. In this method we have to ensure there are bandgap effects caused by the mushroom structure, so the substrate is used to compare with the mushroom structure. Figure 2.11 shows a dipping of the

S21 from 8.2GHz to 9.5 GHz, indicative of a bandgap over that frequency range. Figure 2.11 can be compared to Figure 2.7, from which it is clear that the bandgap region of the dispersion diagram and the dip range of the S-parameter diagram are almost the same. The main purpose of using S-parameter measurement is to compare with the theoretically obtained dispersion diagram, which is hard if not impossible to measure in reality. The S-parameter connects theoretical simulations with reality. The effects of the electromagnetic bandgap are thus indirectly manifested by S-parameter measurements, thereby allowing us to prove the correctness of the dispersion diagram in terms of the bandgap effects.

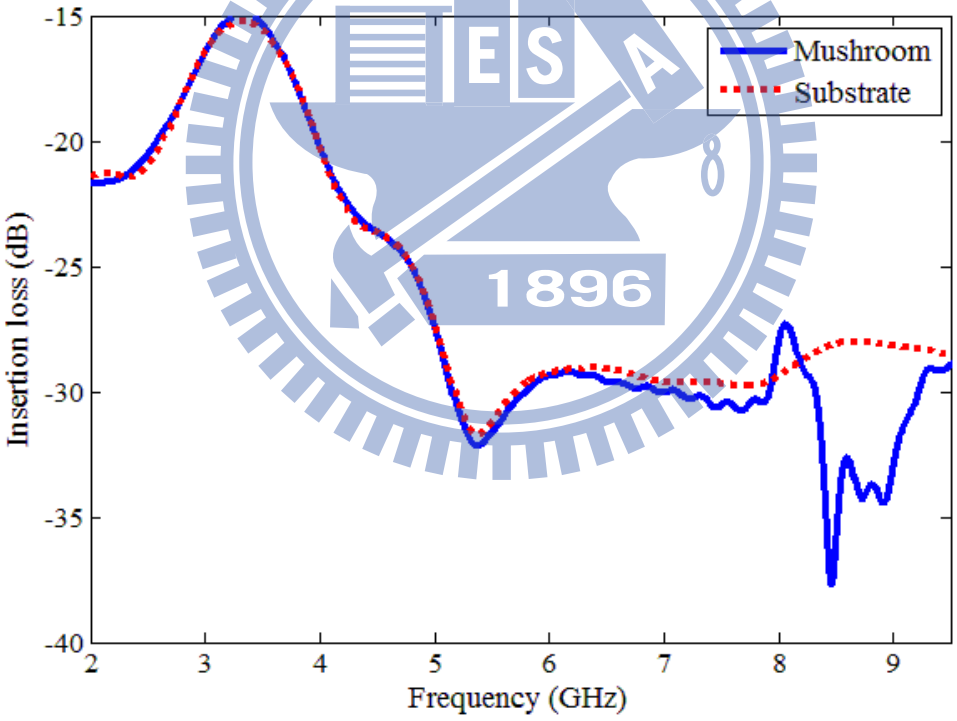

Figure 2.11 S-parameter simulation of mushroom structure and substrate

Chapter 3 Mushroom structure with lumped element

3.1 Introduction

After the characteristics of the mushroom structure had been studied, we know that the frequency range of the electromagnetic bandgap (EBG) is determined by the capacitance and inductance, calculated by the equivalent circuit model. As mentioned before, we can shift this EBG down in the spectrum, by increasing the values of the capacitance and/or inductance. There had been previous works [9] and [10] on modifying the original mushroom structure so as to lower the EBG, thereby making the structure more electrically compact. Although the bandgap can be moved to a lower frequency range by the method of applying interdigital capacitors or meander lines, the design procedure for achieving the exact desired frequency band could be difficult, or at least, non-systematic. So we propose the idea of a straightforward but yet systematic approach of using lumped elements to shift down the frequency band The chief advantages of inserting lumped elements are that lumped elements are usually much smaller than the mushroom structure, and thus easier to design. The size range of the lumped element, SMD capacitor, is from 0402 to 0805, which is smaller than the mushroom structure. Moreover, exact values of the capacitance can be applied by lumped elements instead of interdigital capacitors or meander lines calculated by the equivalent circuit model that can provide only imprecise values. As such, the procedure for designing a compact mushroom structure is more straightforward and thus easier by using lumped elements instead of tuning the value of the equivalent capacitance or inductance through the shapes and dimensions of physical structures.

For those reasons, we initial tried to perform simulation studies with the CST software. Unfortunately, it seems the CST software is unable to produce the effects produced by lumped elements. It means in CST simulation software, insertion of lumped elements is not capable of obtaining the result to prove our hypothesis (assumption). There were initially two possible explanations for this: either our assumption is not correct, or the lumped element cannot be taken into account by the eigen-mode solver in CST simulation software. To break this contradictory deadlock between the hypothesis and CST simulations, we turned to the eigen-solver of the HFSS simulation software for the decider, leaving only the S-parameter simulations of a finite two-port version with lumped elements to the CST software, thereby comparing with the eigen-mode solver results of the HFSS software.

The results of the dispersion diagram and S-parameter diagram by HFSS and CST respectively will be shown in the next sections, and we will show how the electrical size is affected by the other parameters such as the width of the patches, the gap between them, the height of the substrate, and the radius of the via, and then compare the effects of these parameters with those of the lumped elements.

3.2 **Equivalent circuit with lumped element**

An improved equivalent circuit model had been derived in Section 2-2. Its associated formulas there could predict the dispersive behaviors of the TM modal waves more accurately than those by the original unmodified circuit model representation. In this section, we will ride on the waves of that improved model to derive the equivalent circuit, this time with lumped elements. The thoughts behind the derivation are straightforward: we think of the lumped elements as being inserted to the other system, mushroom structure, instead of just parallel to the capacitance between adjacent patches. So we combine the total capacitance derived by Eq. (1.5) and lumped

element into a new total capacitance, shown in Eq. (2.1).

$$C'_{total} = C_{total} + C_{lumped} \tag{2.1}$$

In this research we use the SMD capacitor as the lumped element. We did not use any inductor in this research. So Eq. (2.2) is the same as Eq. (1.10)

$$l_{total} = l_{sheet} + l_{via} \tag{2.2}$$

As long as we have the value of the inductance and capacitance from the equivalent circuit, the modified reactance Z' can be derived from Eq. (1.14), shown in Eq. (2.3).

$$Z' = \frac{j\omega L_{total}}{1-\omega^2 L_{total} C'_{total}} \tag{2.3}$$

In the same way, we can derive the propagation formula of TM and TE waves, shown in Eq. (2.4) and Eq. (2.5).

$$k'_{TM} = \frac{\omega}{c}\sqrt{1-\frac{Z'^2}{\eta^2}} \tag{2.4}$$

$$k'_{TE} = \frac{\omega}{c}\sqrt{1-\frac{\eta^2}{Z'^2}} \tag{2.5}$$

Now that the relationships of the TM and TE waves with lumped elements are derived, we can use Eq. (2.4) and Eq. (2.5) to generate the dispersion diagram and compare it with the one obtained by the HFSS simulation software in the next section.

3.3 **Dispersion diagram with lumped element**

3.3.1 Simulation process

As mentioned, the dispersion diagram of the mushroom structure with lumped elements, herein referred to as compact mushroom structure, cannot be obtained by CST simulation software. We use the HFSS simulation software to get the dispersion diagram as usual. The master-slave process is the same as that laid out in chapter 2, but there is a little difference in the way the lumped element is inserted in HFSS. In order to use the master-slave boundary to create the periodic boundary, we insert the lumped element boundary as a capacitor between patches and the master-slave boundary. This results in an irreducible unit cell model of the compact mushroom structure. The four solid square patches around the central patch represent lumped element boundaries, shown in Figure 3.1 (a), and they will also be inserted between the master-slave boundary walls and the central patch, shown in Figure 3.1 (b).

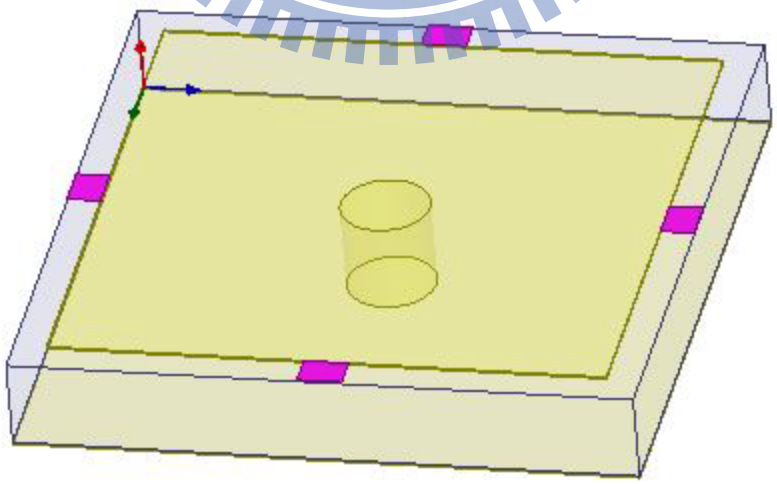

(a)

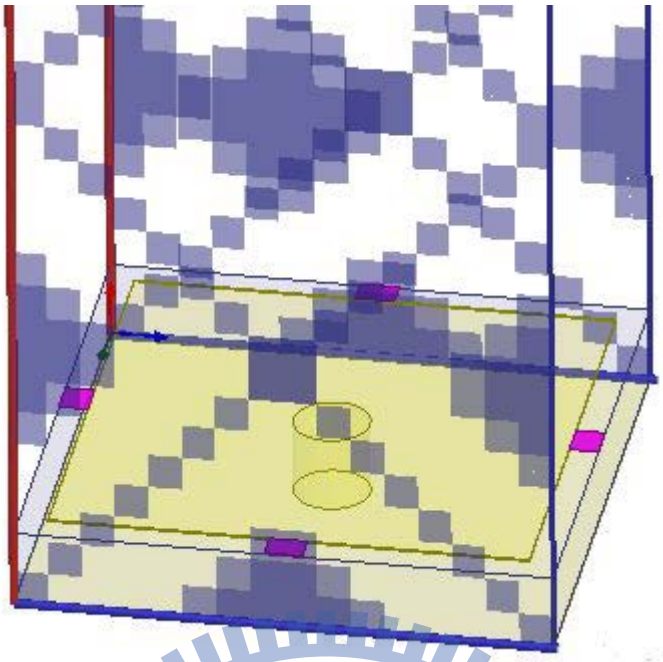

(b)

Figure 3.1 (a) The mushroom structure with lumped element. (b) The mushroom structure with lumped element and master-slave boundary.

In this unit cell, we found an interesting result in the HFSS simulation software. As we introduced before, the lumped element boundary is inserted between the patch and master-slave boundaries, and it means there are infinite number of other mushroom cells behind the master-slave boundary including the lumped element boundary along the x and y axes. As the lumped element boundary is inserted between the patch and master-slave boundary, it is imaged by another lumped element boundary just behind the master-slave boundary. Then the software will take this situation as two series lumped element boundaries. It also means if we want to insert 1pF capacitor between adjacent patches, we cannot just set 1pF value for the lumped element boundary, but instead we have to set 2pF value for the lumped element boundary because the lumped element boundary would be treated as two series lumped elements in HFSS simulation software. This assumption can be proven by S-parameter measurement in the following section.

3.3.2 Simulation result with lumped element

First of all, we insert 1pF capacitance of lumped element boundary to the mushroom structure. As mentioned before, the 1pF lumped element boundary will be ‘seen’ as 0.5 pF in HFSS Eigen-solver mode. The dimension is the same as Figure 2.8 in Section 2-4. The result is given in Figure 3.2 (a), in which the solid and dotted lines represent TM and TE mode respectively. In addition we insert 2pF lumped element to the mushroom structure in HFSS simulation software, as shown in Figure 3.2 (b). These two results of inserting 0.5pF and 1pF in practice can be proven by S-parameter measurements. Then by combining Figure 2.8 and Figure 3.2 (a) with Figure 3.3, we can see that the TM wave is shifted down by about 3GHz after inserting the lumped elements in the same mushroom structure.

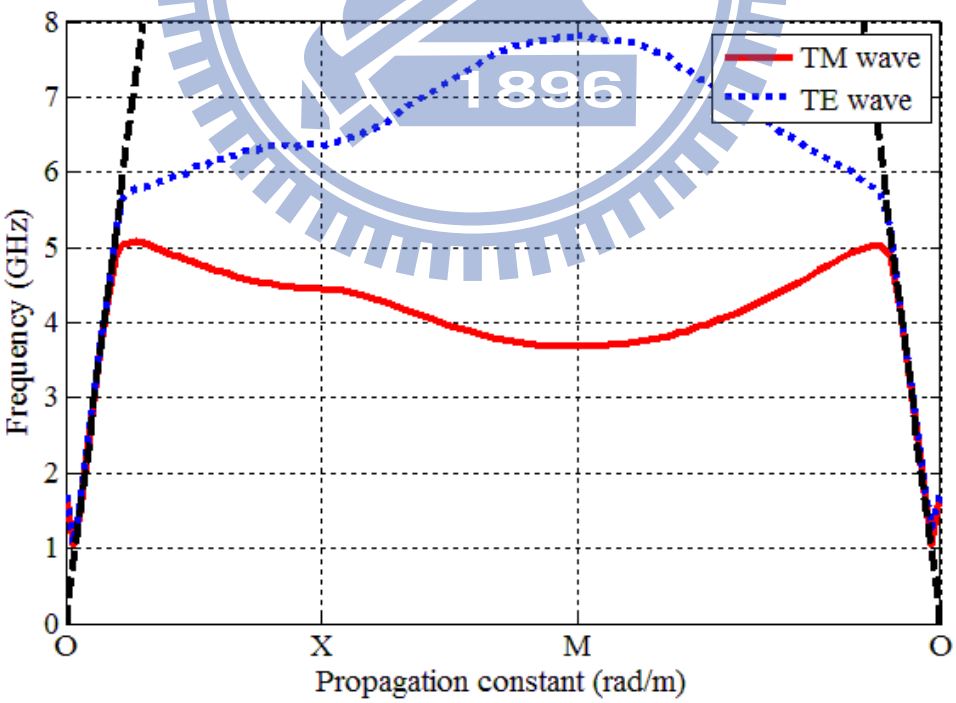

(a)

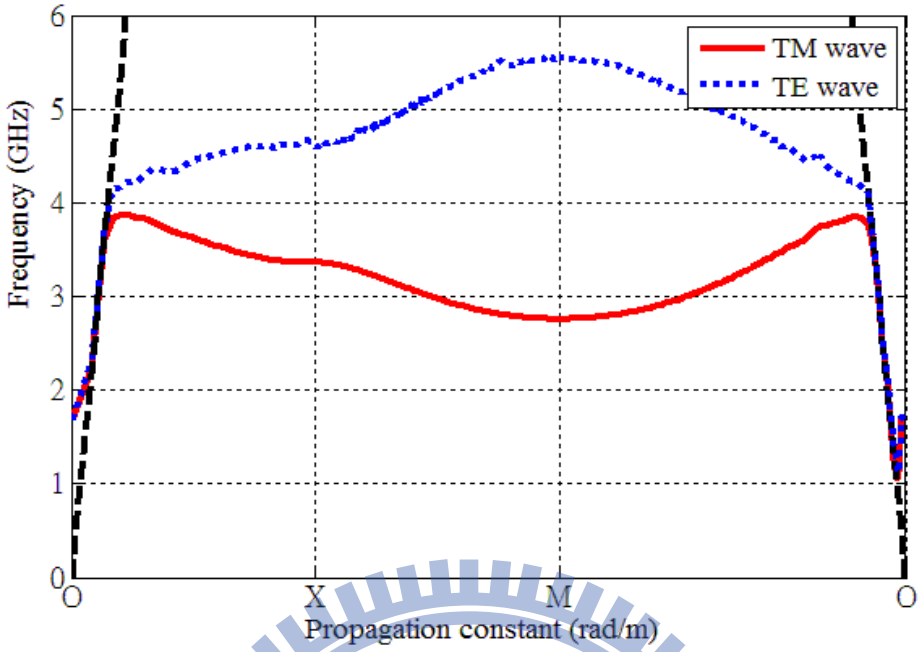

(b)

Figure 3.2 (a) Dispersion diagram with lumped element 0.5pF. (b) Dispersion diagram with lumped element 1pF.

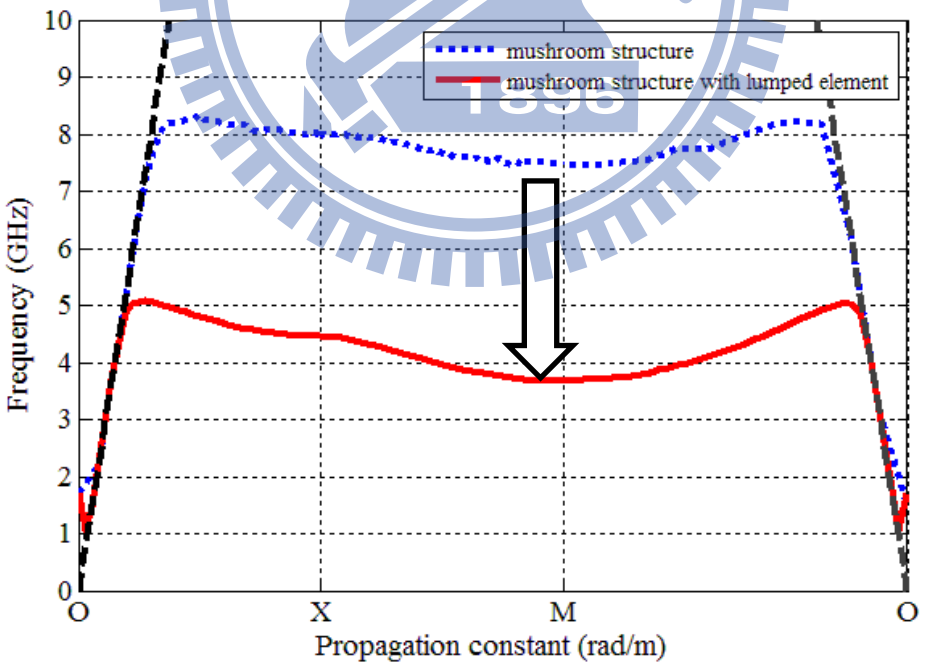

Figure 3.3 The TM mode of mushroom structure and compact mushroom structure

Combining Eq. (2.4) and Eq. (2.5) the dispersion diagram of the mushroom structure with lumped element can be drawn, for just the O→X path, shown in Figure 3.4. The solid line and solid line with square markers represent TE and TM waves by HFSS simulation software with 0.5pF lumped elements respectively. The dotted line and dotted line with triangular markers represent TM and TE waves obtained by the equivalent circuit model with 0.5pF lumped elements respectively. We can see that the TM waves are not matched perfectly after the turning point, but the TE waves can be predicted as the same as HFSS simulation software. Nevertheless, Figure 3.4 shows that the trends of using lumped elements can be predicted by the equivalent circuit model. Although the TM wave is not matched perfectly, it must be made sure that no propagation is permitted within the frequency range of the resultant bandgap predicted by the circuit model. So the bandgap range should occur from the highest frequency of the TM wave to the lowest frequency of the TE mode behind the light line. We can compare the dispersion behavior of the TM waves produced by HFSS simulation with the one predicted by the equivalent circuit conveyed by Eq. (2.4) and Eq. (2.5). It is seen that both turning points have the same value in Figure 3.4. It means we can still predict the right bandgap by the equivalent circuit model even by inserting lumped elements.

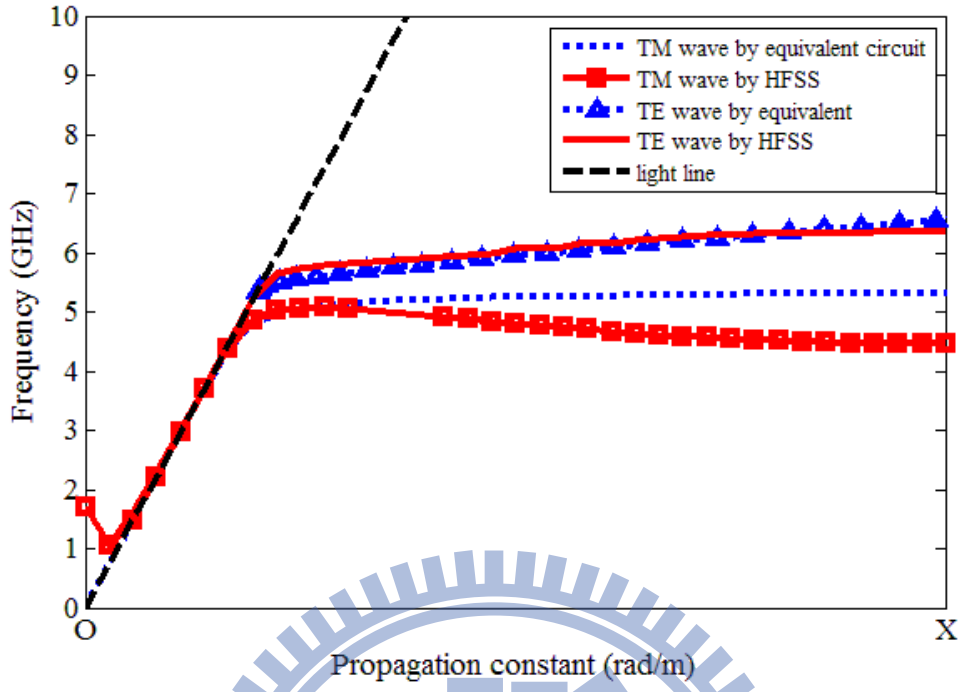

Figure 3.4 TM and TE wave produced by different method in O-X part

3.4 **S-parameter diagram with lumped element**

In this section, we will use S-parameter simulations to prove the effects of the mushroom structure with lumped elements, and thereby demonstrate the validity of the simulation results obtained by HFSS eigen-solver as discussed in Section 3.3.2. As mentioned, lumped elements could not be detected in the Eigen-solver of the CST simulation software for generating the dispersion diagram. Hence, we mooted the other alternative of using the HFSS simulation software and equivalent circuit model to obtain the dispersion diagram. But we want another objective method to ensure the correctness of the HFSS simulation software and the equivalent circuit method. This S-parameter method is just like in Section 2-5, but the mushroom structure is now inserted by lumped elements each with capacitance of 0.5 pF in the CST simulation software. On the other hand, master-slave boundary is not needed in these S-parameter simulations, since all boundaries are open to emulate the real world. And

each lumped element is now perceived as a unique unit cell instead of a combination of two series lumped elements, shown in Figure 3.5.

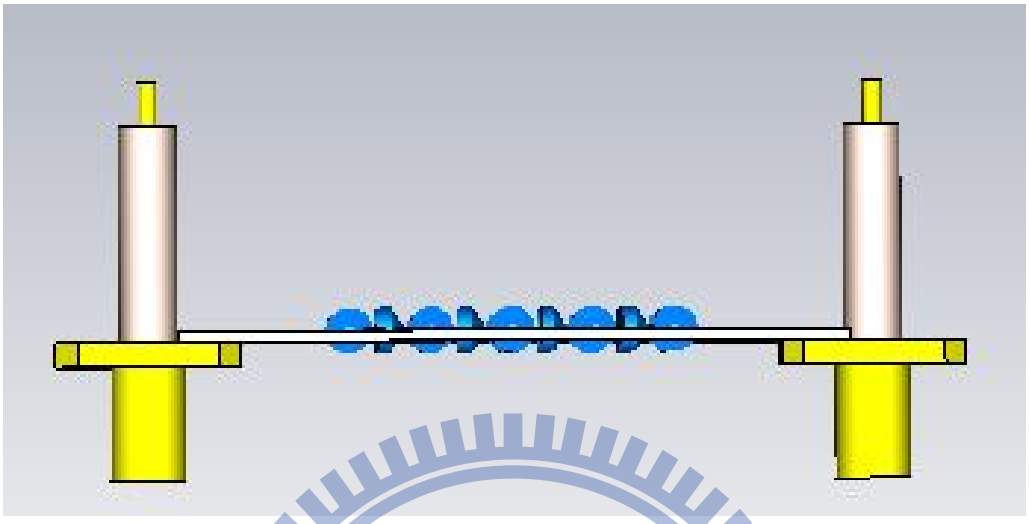

(a)

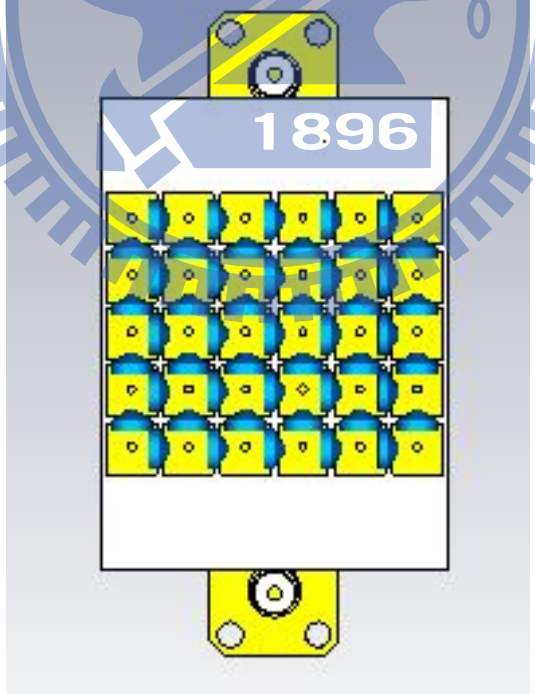

(b)

Figure 3.5 (a) The cross-section view and (b) the top view of S-parameter measurement with lumped element

By the method of Figure 3.5, the S-parameter simulation result can be observed by CST. Figure 3-6 shows the effects after inserting the lumped elements to the mushroom structure via a graph of the insertion loss against the frequency. Figure 3.6 is the same as Figure 2.1, but there are two extra curves. The solid-dotted line is for the mushroom structure, the dashed-line is for the substrate alone (RO4003 and thickness of 0.8mm) with no any copper, and the solid line and dotted line are for the mushroom structure with lumped elements of capacitances 0.5pF and 1pF respectively. We can see that the frequencies at which dips occur in the curves (indicative of the bandgap center frequencies) with lumped elements of capacitances 0.5pF and 1pF are shifted down to about 5GHz and 4GHz, whereas the bandgap center frequency of the original mushroom structure without any lumped element still stays at 8.2GHz. In this case, the effects of the lumped elements can be proven by S-parameter simulations. This result can be compared with Figure 3.2, for which both bandgap center frequencies simulated by HFSS and CST simulation software are similar at 5GHz and 4GHz by inserting 0.5pF and 1pF capacitors in CST, but 1pF and 2pF in HFSS simulation software. Figure 3.6 proves the assumption in Section 3.3.2, but the bandwidths of both bandgaps do not match very well. An explanation for this is that the dispersion diagram is characterized by three parts and infinite number of unit cells, so the dispersion diagram analysis is more accurate than S-parameter simulation. Nonetheless, we cannot deny the contributions of S-parameter simulations. So far, S-parameter simulations and measurements are the quickest ways to observe the bandgaps effects of compact mushroom structure effects, theoretically and in practice.

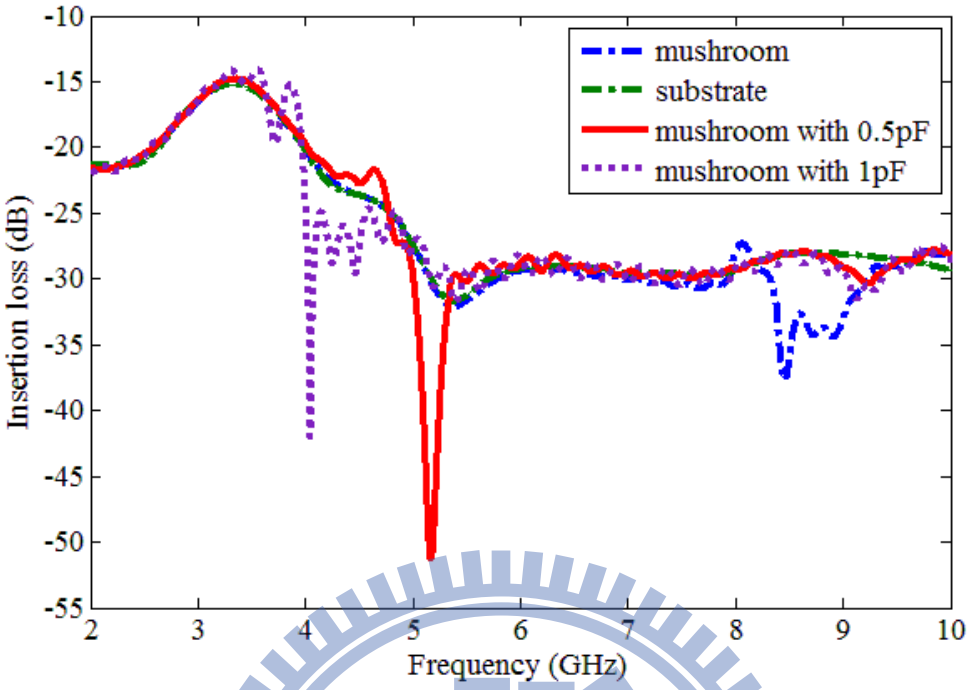

Figure 3.6 S-parameter simulation results of mushroom structure, substrate, and mushroom structure with 0.5pF and 1pF.

3.5 **Measurement results**

In this section, we will show the measurement result by the S-parameter method. Figure 3.7(a) and Figure 3.7(b) are the top views of the mushroom structure and the compact mushroom structure with 1pF capacitors respectively. First we measure the original mushroom structure without any lumped elements, and then solder 1pF capacitors onto the same mushroom structure. Figure 3.8 gives the results of the S-parameter measurement. We can see that the curve for the substrate has a little difference from those of the mushroom structure and the mushroom structure with 1pF capacitor. Although the permittivities of the substrates used for all structures are supposedly the same (being that of RO4003), these dielectric boards were not produced at the same time. The curve in Figure 3.8 for the substrate alone is used to demonstrate the dip at 6GHz as a common effect on the RO4003 substrate, as opposed particularly to being produced by the mushroom structure. In Figure 3.8, the

solid line is for the bare substrate, the dotted line is for mushroom structure without any lumped element, and the solid-dotted line is for the compact mushroom structure with 1pF capacitor. As observed, aside from the common one at 6GHz attributed to the substrate as explained above, there are dips at 9GHz and 4GHz produced by the mushroom structure and the compact mushroom structure with 1pF capacitor respectively. The simulation and measurement results are compared favorably by Figure 3.6 and Figure 3.8. As explained, the comparison between these two figures excludes the dip at 6GHz produced by the practical substrate or surroundings.

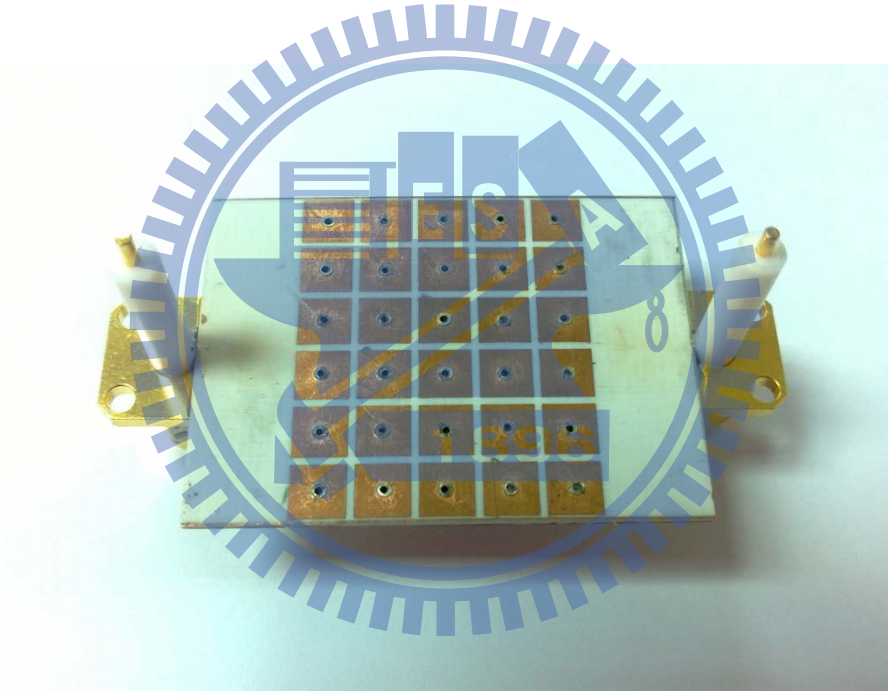

(a)

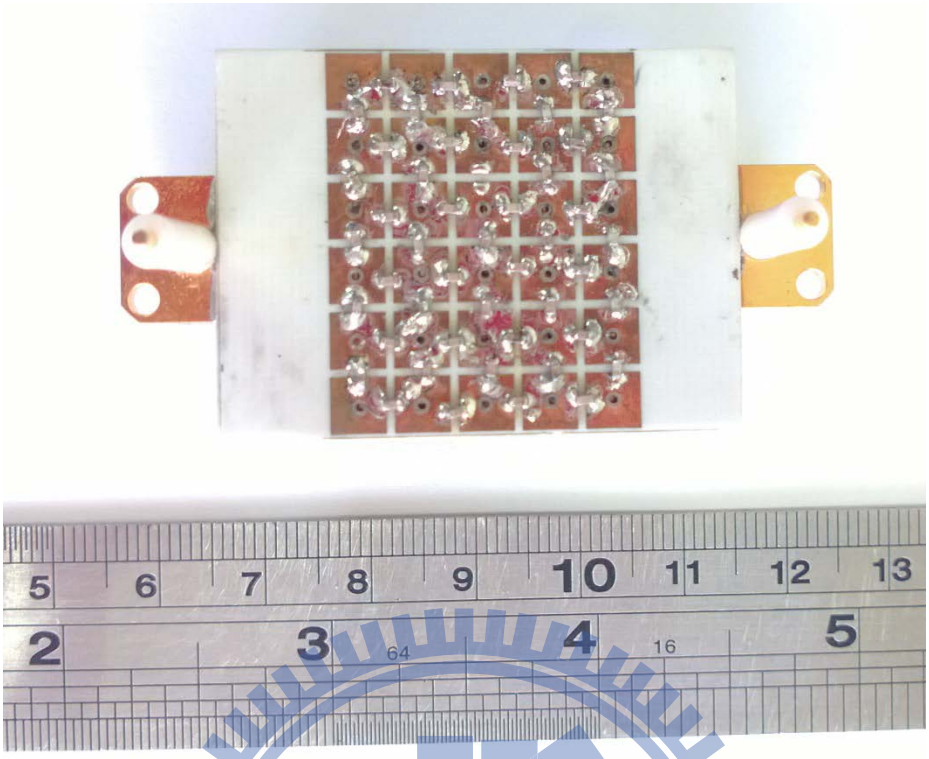

(b)

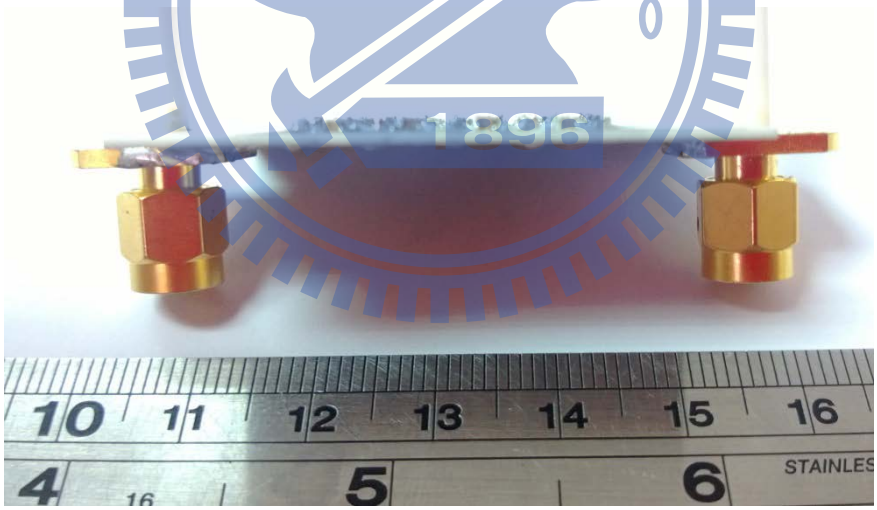

(c)

Figure 3.7 (a) The top view of mushroom structure and (b) mushroom structure with 1pF capacitor (c) the side view of mushroom structure with 1pF capacitor.

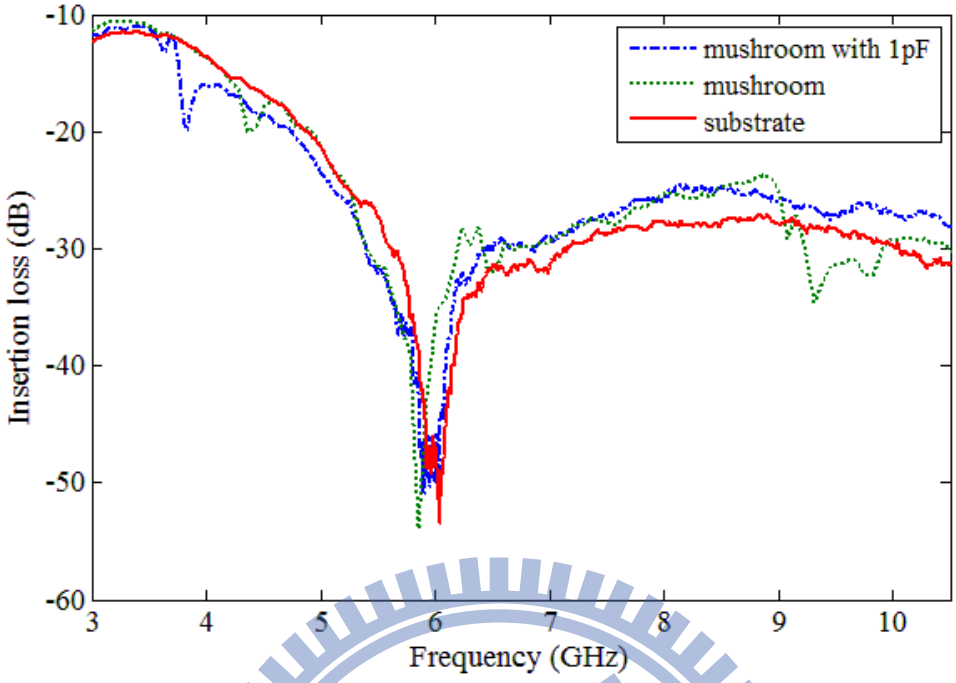

Figure 3.8 The measurement results of substrate, mushroom structure, and mushroom structure with 1pF capacitor.

Chapter 4 Small Antenna with mushroom structure

4.1 Introduction

As mentioned, we know the mushroom structure can suppress surface waves in the bandgap, as observed by the dispersion diagram. And we introduced the other two methods to prove the correctness of the bandgap, such as the equivalent circuit method and by S-parameter measurements. We also know that the microstrip antenna will excite surface waves. Surface waves bound to the dielectric-air interface will interfere with the radiation in free space. Moreover, the surface wave will reduce the energy from the excitation, as shown in Figure 4.1. In this chapter, we will first introduce and motivate the concept as to why the EBG structure can improve the efficiency, and then use the patch antenna to combine with mushroom structure, thereby comparing between the cases with and without the mushroom structure. Furthermore, the small antenna will be designed to combine with the compact mushroom structure, from which it can be used to prove whether or not surface waves can really be suppressed by the compact mushroom structure.

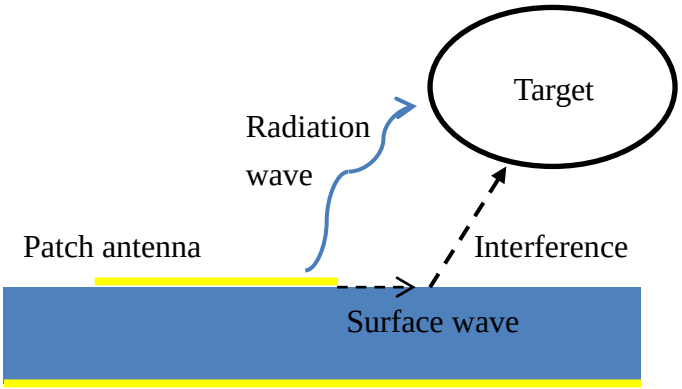

Figure 4.1 Surface wave exicited by patch antenna

4.2 **Radiation efficiency**

Radiation efficiency is defined by IEEE as "The ratio of the total power radiated by an antenna to the net power accepted by the antenna from the connected transmitter." If all the input power appeared as the radiated power; that is $P_{in} = P_r$, the radiation efficiency is 1, or 100% [13]. Hence, the radiation efficiency is defined as Eq. (4.1). We all know losses always exist in any practical antenna. The input power thus gets distributed in the form of the radiated power, surface wave power, and dissipation in the conductor and dielectric, as expressed in Eq. (4.2) [13]. We also know that the conductivity and dielectric losses, P_c and P_d, depend on the characteristics of the material, which are virtually unchangeable. The radiated power is defined by the antenna, so the only factor that we can use to improve the radiation efficiency is through the surface power. As mentioned, the surface wave can be suppressed by the EBG structure, or mushroom structure. So assuming the other factors are maintained in Eq.(4.2), and $P_{surface}$ is decreased by the mushroom structure, then the radiation efficiency will be increased.

$$e_r = \frac{P_r}{P_{in}} \tag{4.1}$$

$$e_r = \frac{P_r}{P_r + P_c + P_d + P_{surface}} \tag{4.2}$$

4.3 **Patch antenna with mushroom structure**

There have been substantial amounts of research put into investigating how the efficiency of an antenna can be improved by adding an EBG structure, such as [14] and [15]. In the last chapter, we used three different methods to obtain the location of the bandgap in the spectrum. In the beginning of Section 4-3, the patch antenna will

be designed to combine with the original mushroom structure introduced in Figure 2.8. Figure 4.2 shows the frequency response of the return loss of the patch antenna and the patch antenna with the mushroom structure. The resonant frequency of the patch antenna and the patch antenna with the mushroom structure are 9.1GHz and 9.28GHz respectively. We will also compare the radiation efficiency of both antennas, shown in Figure 4.3. When the patch antenna is combined with the mushroom structure, the efficiency is improved. This experiment is the initial work of producing antennas to prove the effects of adding the mushroom structure. Then in the following section, we will design the patch antenna with a lower operation frequency to be combined with the mushroom structure with lumped elements inserted.

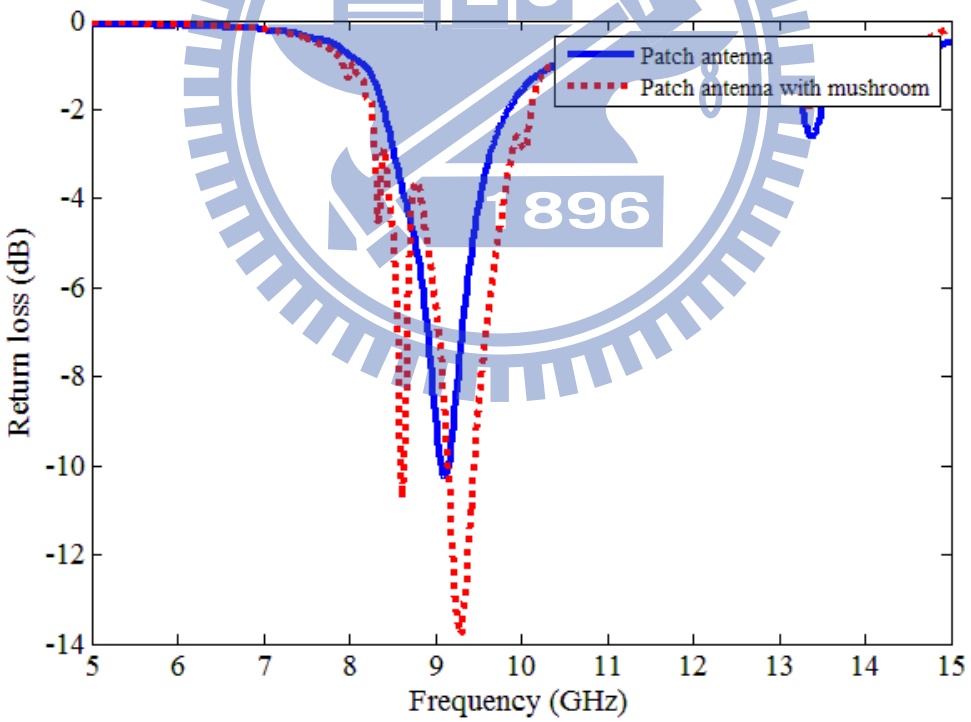

Figure 4.2 return loss of two patch antennas.

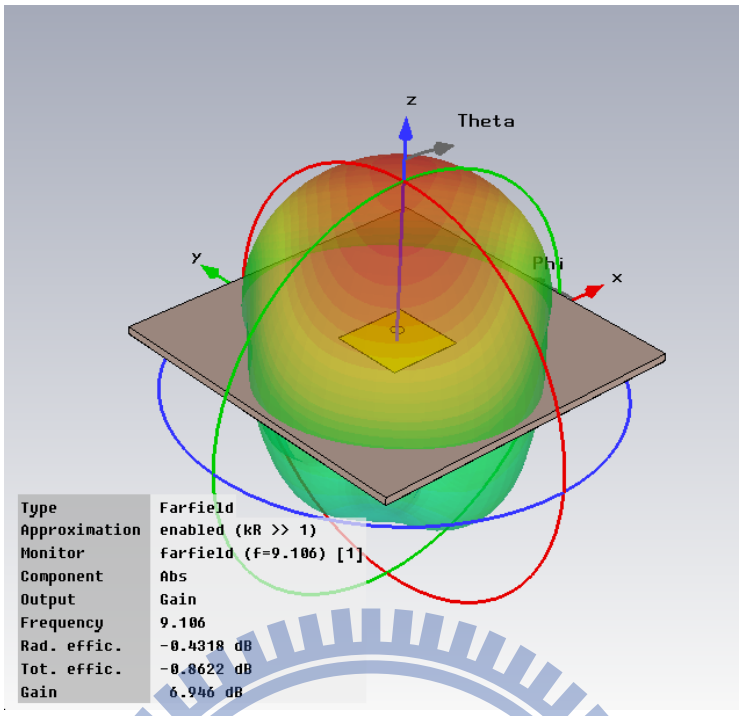

(a)

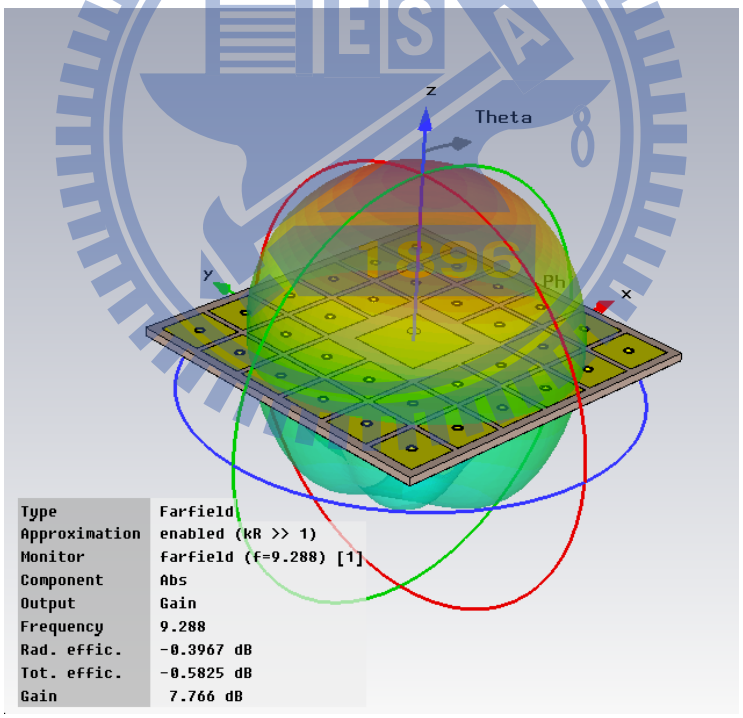

(b)

Figure 4.3 (a) The far-field simulations of patch antenna and (b) patch antenna with mushroom structure

4.4 **Patch antenna with compact mushroom structure**

In this section, we have already taken the patch antenna as the example to improve the efficiency by using the mushroom structure. Furthermore, a patch antenna will be designed to prove the effects of the mushroom structure with lumped elements at the lower frequency. As mentioned in Figure 3.2 (b), the bandgap of the mushroom structure would be pulled down to a lower frequency range after inserting lumped elements as observed by the dispersion diagram. When 1pF lumped elements are inserted, the TM mode will be shifted from 8GHz to 4GHz, and the bandgap range is from 3.8GHz to 4.2GHz, as shown in Figure 3.2 (b). Then the patch antenna is designed to combine with the mushroom structure with 1pF lumped element at 3.91 GHz. Figure 4.4 shows the variation of the return loss with frequency of the patch antenna and the patch antenna with lumped elements inserted to the accompanying mushroom structure. It is observed that the minima of the return loss for both cases occur almost at the same resonant frequency. In addition, we also compare the radiation efficiency of both cases to see whether or not the bandgap is truly shifted by the lumped element at 3.91GHz. Figure 4.5 shows both the far-field results of the original patch antenna and those of the patch antenna with the compact mushroom structure. For the original patch antenna, its radiation efficiency is –1.209dB, total efficiency –1.217dB, and its gain is 5.996dB, as shown in Figure 4.5 (a). As for the patch antenna with the mushroom structure loaded with 1pF lumped elements, the radiation efficiency is –0.4336dB, total efficiency –0.5832dB, and the gain is 6.822dB, as shown in Figure 4.5 (b).

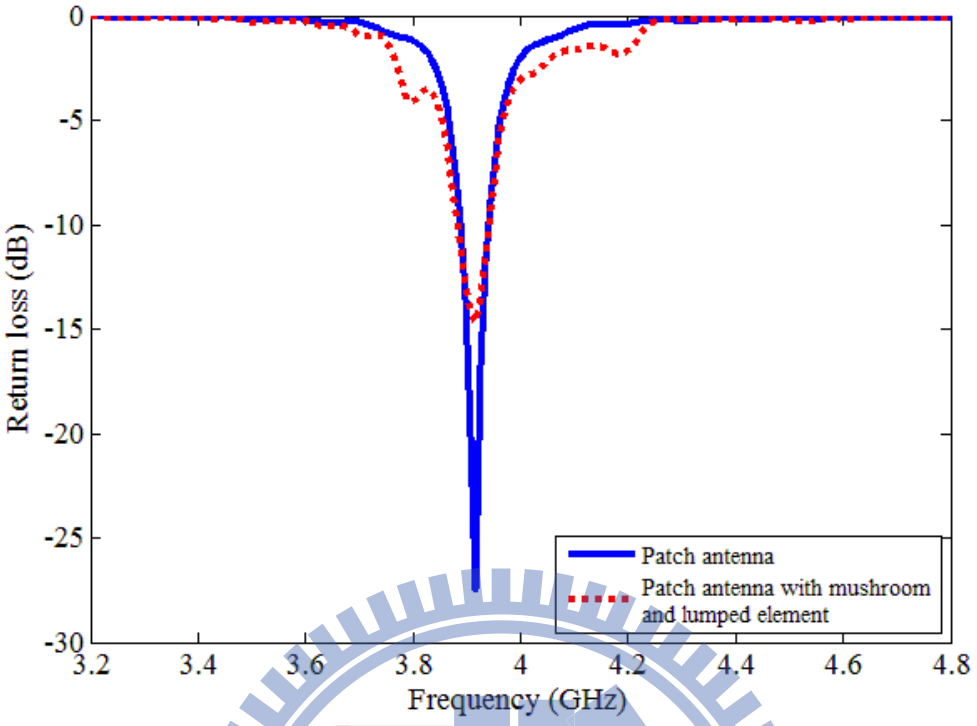

Figure 4.4 Return loss of patch antenna and patch antenna with mushroom structure and lumped element

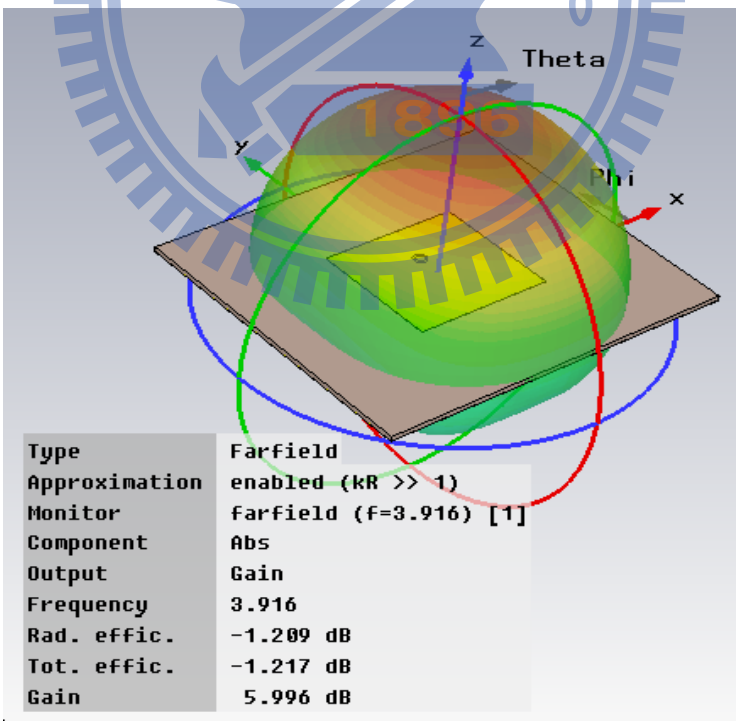

(a)

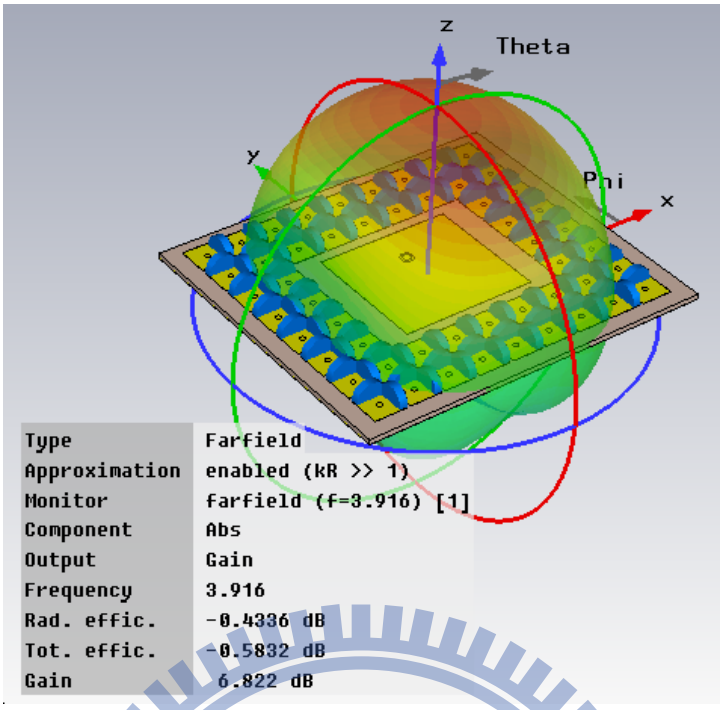

(b)

Figure 4.5(a) The far-field result of patch antenna at lower frequency and (b) patch antenna with compact mushroom structure.

Table 4-1 shows the brief result to compare both antennas with and without mushroom structure. We can get some conclusion from comparison. Although the idea of using lumped element to pull down the bandgap can be derived or observed by HFSS simulation result, equivalent circuit prediction, and S-parameter simulation in CST simulation software. We never use this structure, with lumped element, for applications such as antenna before. Section 4-3 provided the experiment to use the mushroom structure with lumped element to combine with patch antenna. We know the patch antenna is one of the simplest structures in the antenna engineering. So we take patch antenna for example, hoping to find any improvements after combining with lumped element inserted mushroom structure. Fortunately, these results show the good trends in any performance, such as radiation efficiency, total efficiency, and the antenna gain. According to table 4-1, we really have good results in patch antenna by using compact mushroom structure with lumped element. Then we assume that

compact mushroom structure can combine with any microstrip antenna to improve its performance at the particular frequency. In the following section, the small and complex antenna will be designed to combine with compact mushroom structure. If it works, we will have high performance antenna, instead of restriction by larger EBG structure.

Table 1 Comparison of patch antenna with both mushroom struxture and compact mushroom structure

	Rad. efficiency	Tot. efficiency	Gain dB)
patch antenna (9.1GHz)	90.5%	82%	6.946
patch with mushroom (9.2GHz)	91.27%	87.45%	7.766
patch antenna (3.9GHz)	75.7%	75.56%	5.996
patch with mushroom and lumped element (3.9GHz)	90.5%	87.43%	6.822

4.5 **Small antenna with mushroom and lumped element**

As mentioned, the main idea is proposing the compact mushroom structure to combine with the small antenna. In this section, we will use the concept of metamaterial technology to design the compact antenna. Figure 4.7 shows the properties of metamaterial antenna, it can also called CRLH antenna. The dispersion curve on the $\beta > 0$ side is the right-handed mode, while the dispersion curve on the $\beta < 0$ side is the left-handed mode. The electrical size of conventional antenna is restricted by its physical dimension, but if we can use the region of $\beta < 0$, left-handed mode, the size of CRLH antenna can be reduced [16]. The method of realizing CRLH antenna is using series capacitance, and shunt inductance, like periodic structure or

mushroom structure. So the antenna design is based on mushroom structure.

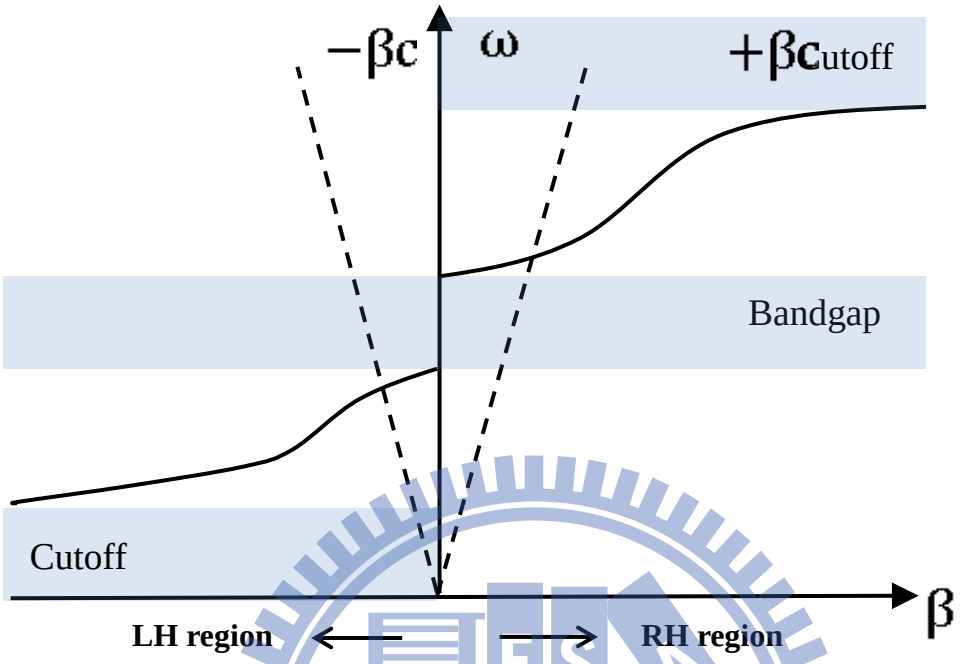

Figure 4.6 Dispersion diagram of right left handed region

Although, we can use more unit cell to get the lower operating frequency by Figure 4.6. Using left-handed modes with indexes more than -1can result in impedance matching issues and low-radiation-efficiency problems [16]. So how to design the exactly number of unit cell are the important skills in CRLH antenna. In this section, the two unit cell CRLH antenna is designed, shown in Figure4.7. This antenna is based on two mushroom structures. However, this mushroom structure has a low-series capacitance between two mushroom structures, calculated by Eq. (1.3). In order to increase the capacitance between two patches, the interdigital capacitor has been added instead of using lumped element [16].However, the concept of antenna design is based on mushroom structure, both two patched are not square, because of considering its matching network. For wireless technology, the antenna is designed at the 5.35GHz, which comfort to standard of 802.11 ac. The dimension of patches a and b are 4.2×5.35 mm, the length of interdigital capacitor L is 3.2 mm, the gap between

interdigital capacitor p is 0.65 mm, the gap between interdigital capacitor and patch g is 0.2 mm, the diameter of via place at the central of patches d is 0.4 mm, the feed line is 50Ω, the substrate is RO4003, the dielectric constant of 3.55 and thickness h of 0.8 mm, and the dimension of substrate $s \times w$ is 40×30 mm. The idea of using interdigital capacitor instead of lumped element is that we want to focus on inserting lumped element to produce the compact mushroom structure exciting the lower bandgap, not for application, and to avoid the confusion of lumped element effects. The electric size of CRLH antenna is $0.28\lambda_o \times 0.095\lambda_o$. Figure 4.8 shows the combination of CRLH antenna and mushroom structure in CST simulation software. Dimension of mushroom structure is the same as Figure 2.8, and use 0.5pF capacitor to shift the bandgap at applicable place to match the resonant frequency of CRLH antenna at 5.35GHz, shown in Figure 3.2 (b)

Figure 3.2

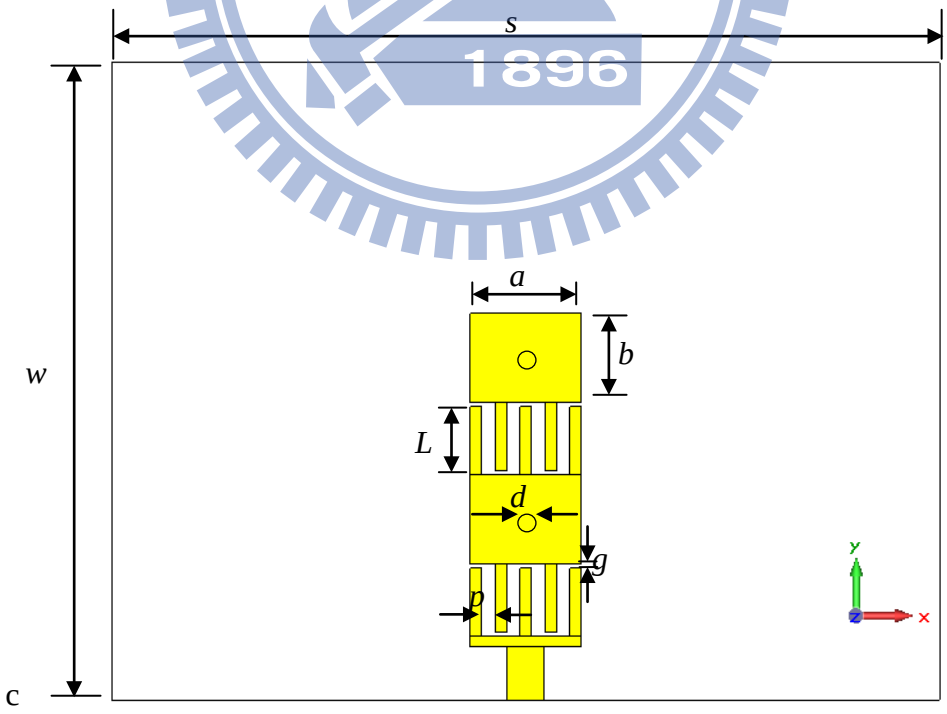

Figure4.7 The top view of metamaterial antenna.

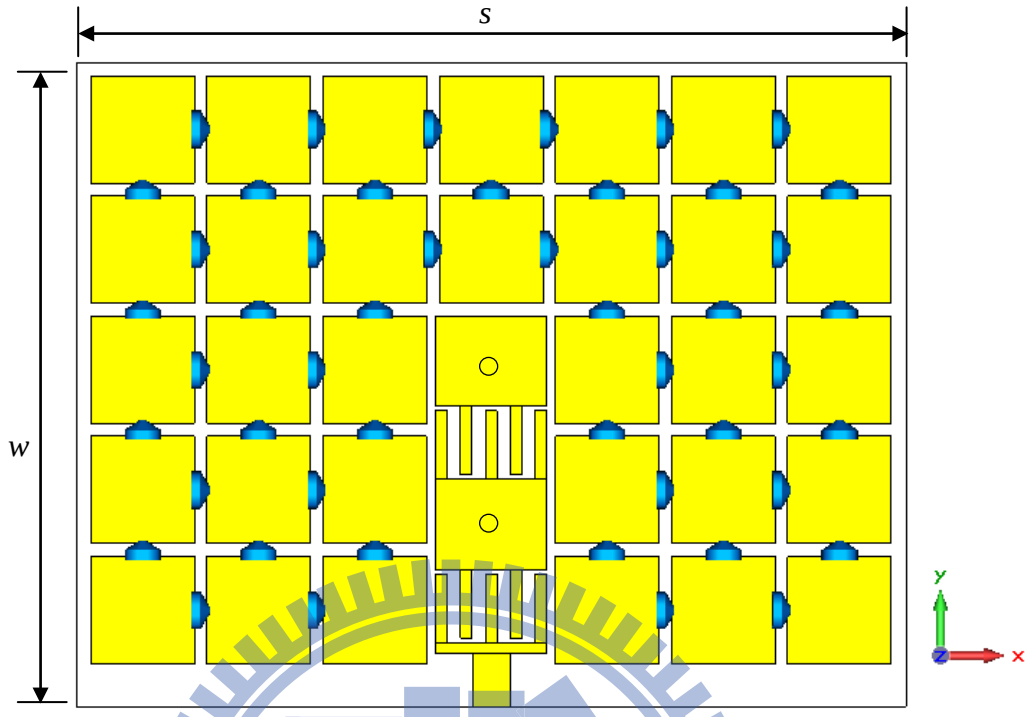

Figure 4.8 Top view of CRLH antenna with mushroom structure and lumped element

Figure 4.9 shows the return loss of small antenna and small antenna with compact mushroom structure. The dotted line and solid line are original antenna and antenna with compact mushroom structure respectively. We can see there are three resonant frequencies at 5.35, 6.92 and 8.81 GHz in original antenna, but the bandgap of compact mushroom structure is only at 5GHz to 5.5GHz between first and second order mode, shown in Figure 3.2 (b). In this case, the only resonant frequency should be analyzed is 5.35 GHz. Figure 4.9 shows that the frequency with compact mushroom structure is shifted to 5.23GHz, but it still close to 5.35GHz and in the bandgap range.

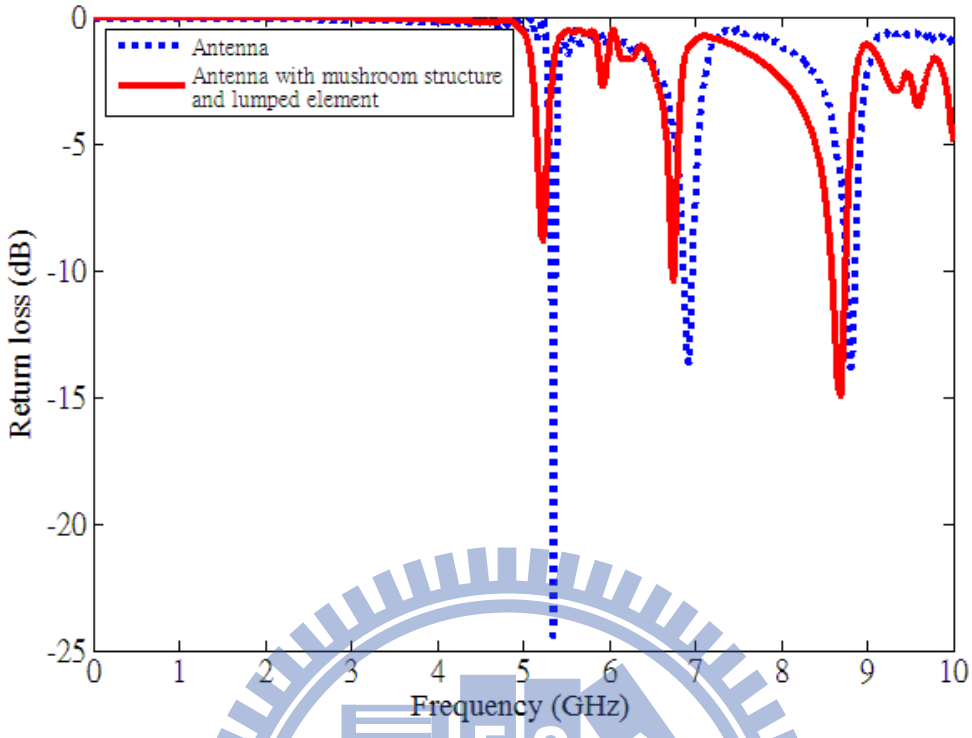

Figure 4.9 Return loss of original antenna and antenna with mushroom structure and lumped elements

Then we will discuss the radiation efficiency after the return loss diagram is compared between antenna and antenna with compact mushroom structure. Figure 4.10 is the far-field pattern of original antenna, and we use the straightly method, linear scaling, to observe both efficiency. The radiation efficiency and total efficiency of CRLH antenna is 0.2916 and 0.2907 respectively. It seems this is not a good antenna, and the antenna gain is 1.176. From Figure 4.10, we know while we pursue to decrease the antenna size, but it also causing the reduction of the antenna's performance. So we use the compact mushroom structure to solve this problem. Figure4.11 shows the performance of antenna after combining with compact mushroom structure. The radiation efficiency is improved from 0.2918 to 0.8064, the total efficiency is increased from 0.2907 to 0.5995, and the gain is raised to 3.648. The performance is improved after inserting compact mushroom structure.

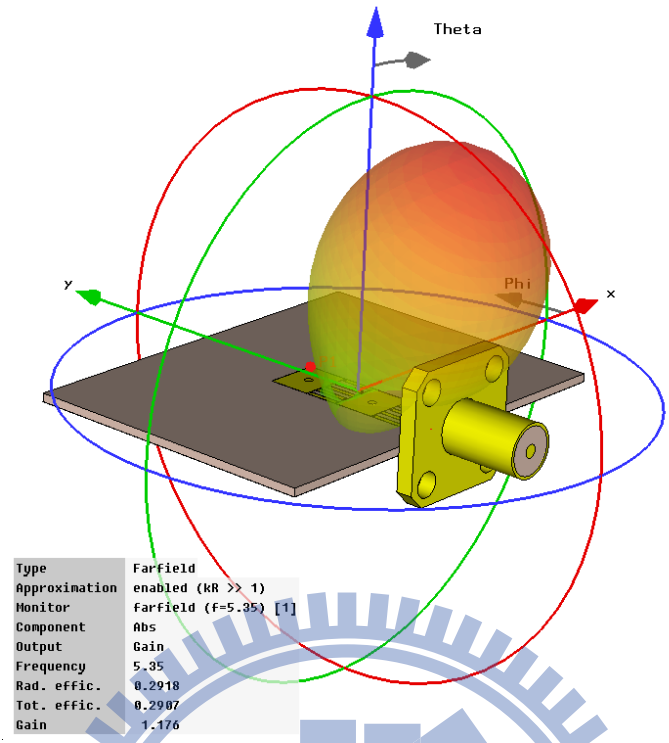

Figure 4.10 Far-field of original antenna

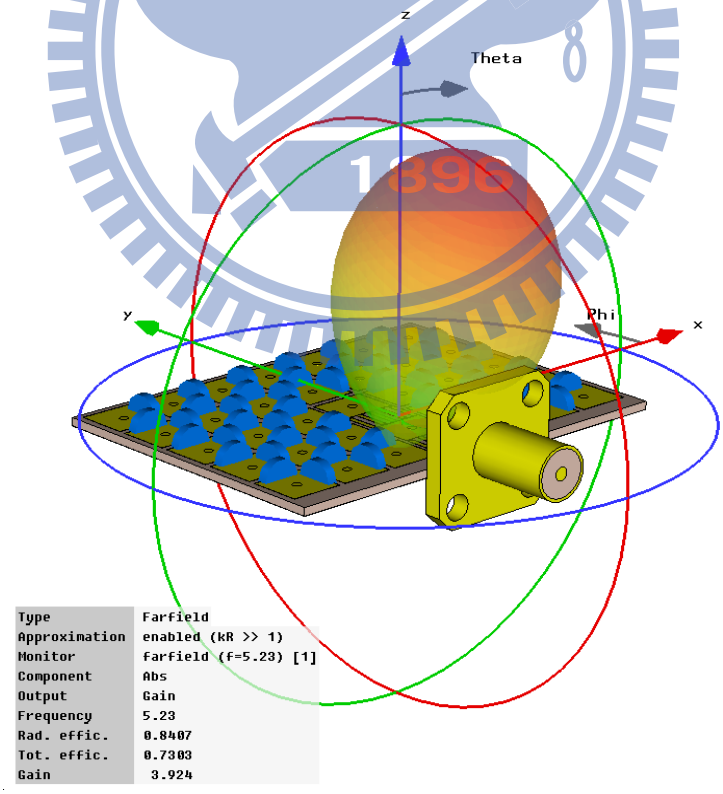

Figure4.11 Far-field of antenna with mushroom structure and lumped element

Table 2 Performace of CRLH antenna and CRLH antenna with compact mushrooom structure

	Rad. efficiency	Tot. efficiency	Gain
Small antenna (5.35GHz)	29.18%	29.07%	1.176
Small antenna with compact mushroom structure (5.28 GHz)	84.07%	73.03%	5.937

In Table 2 Performace of CRLH antenna and CRLH antenna with compact mushrooom structure, we can easily see the improvement after the small antenna combining with compact mushroom structure. But, how can we know that this improvement is realized by compact mushroom structure. Does the original mushroom structure also can enhance antenna's performance? To verify this doubt, we propose another experiment. We use the same CRLH antenna, shown in Figure4.7 to combine with mushroom structure without lumped element, shown in Figure 4.12. Figure 2.8 shows the bandgap of original mushroom structure is from 8.2GHz to 9.5GHz. This bandgap does match to resonant frequency of CRLH antenna at the 5.35 GHz. The return loss diagram result is shown in Figure 4.13. The solid line is small antenna, and the dotted line is small antenna with original mushroom structure. There are still frequency shift after combining original mushroom structure, which resonant frequency is 5.21GHz. It's similar to small antenna with compact mushroom structure. So we can assume that frequency shift is caused by mushroom structure, not lumped element. Figure 4.14 shows the performance of small antenna with mushroom structure. It also demonstrates by linear scaling. Radiation efficiency is 0.2735, total efficiency is 0.2729, and the gain is 1.031. The farfiled result is even worse than CRLH antenna without any EBG structure shown in Figure 4.14. This simulation result proves that the compact mushroom structure can exactly improve antenna's performance rather than other

mushroom structure, which electric size is large and not at the right bandgap.

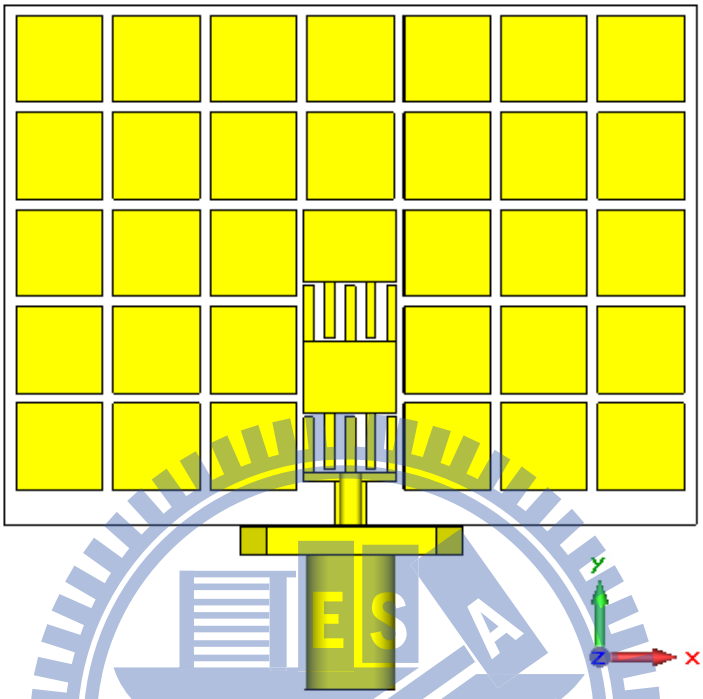

Figure 4.12 CRLH antenna with original mushroom structure

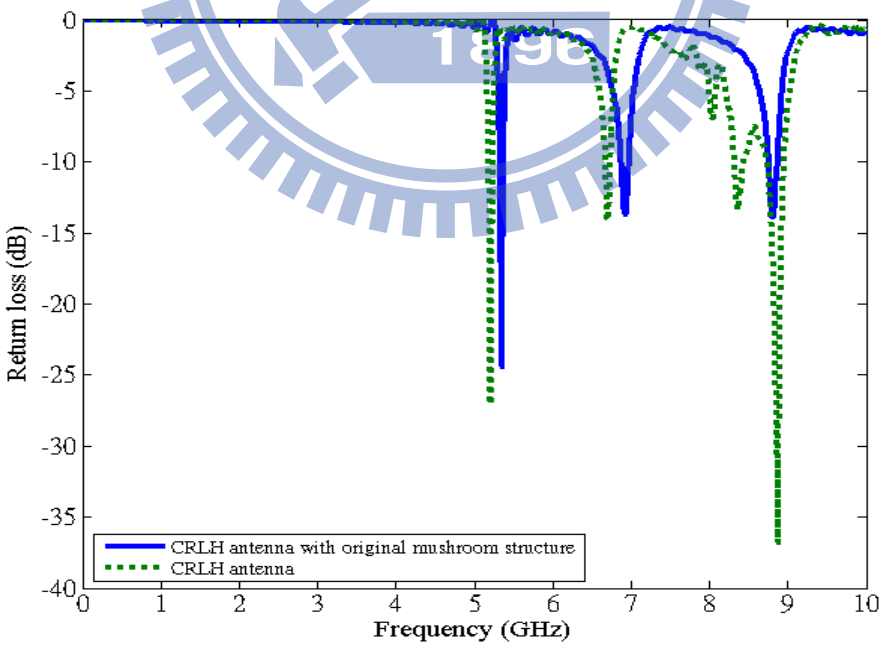

Figure 4.13 Return loss of CRLH antenna and CRLH antenna with original mushroom structure

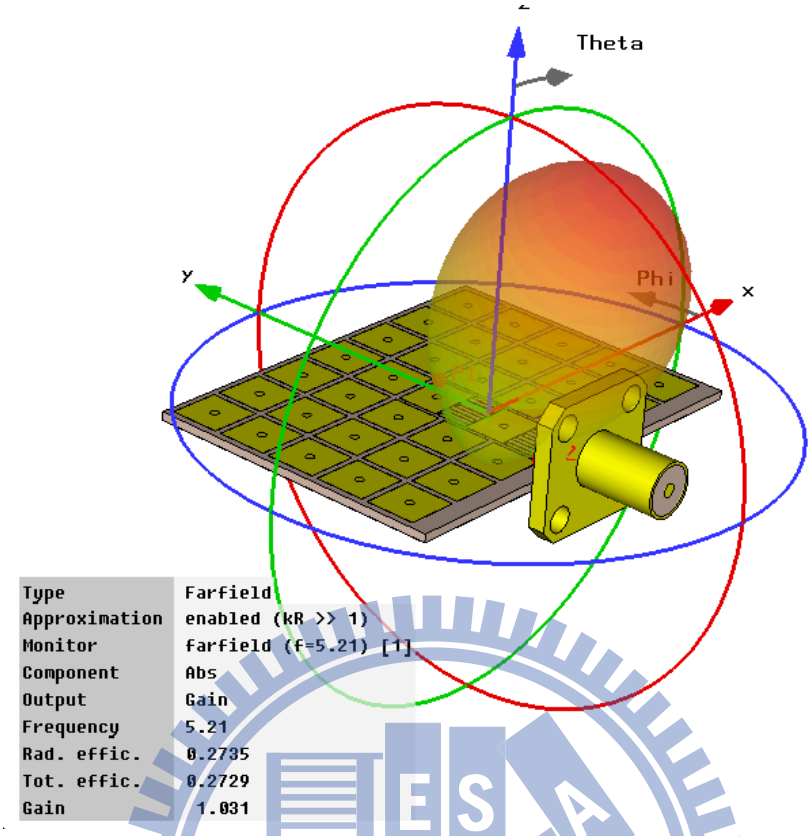

Figure 4.14 Far-field result of CRLH antenna with original mushroom structure

Chapter 5 Measurement results

In chapter 4, the simulation result had been shown that the antenna performance can be improved by compact mushroom structure. So in this chapter, we had fabricated these antennas to observe that the contributions of combining compact mushroom structure

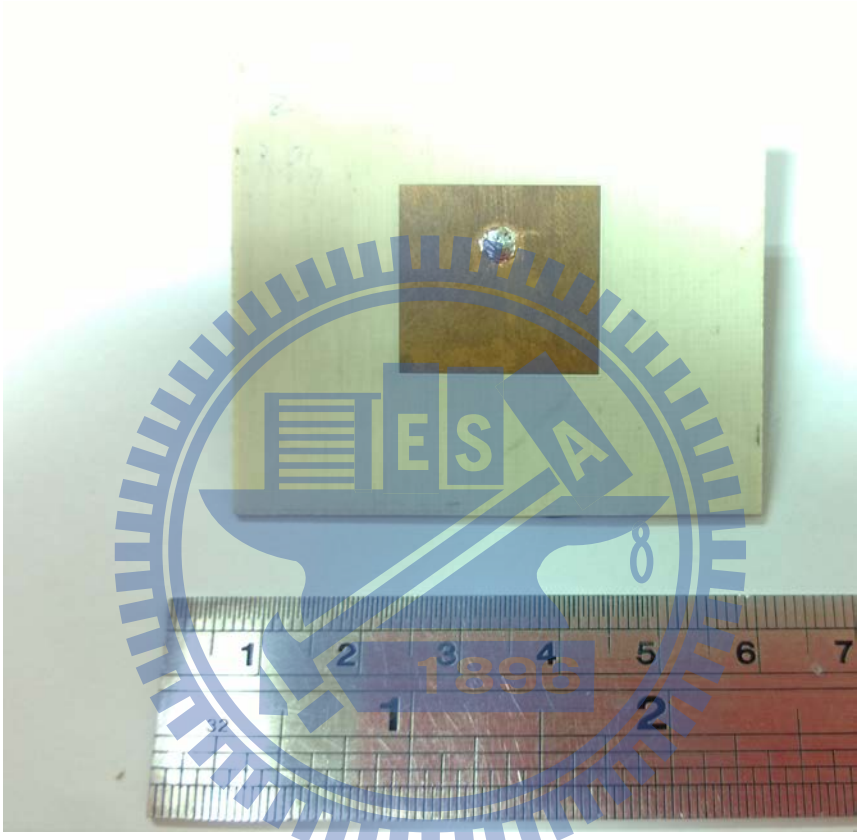

(a)

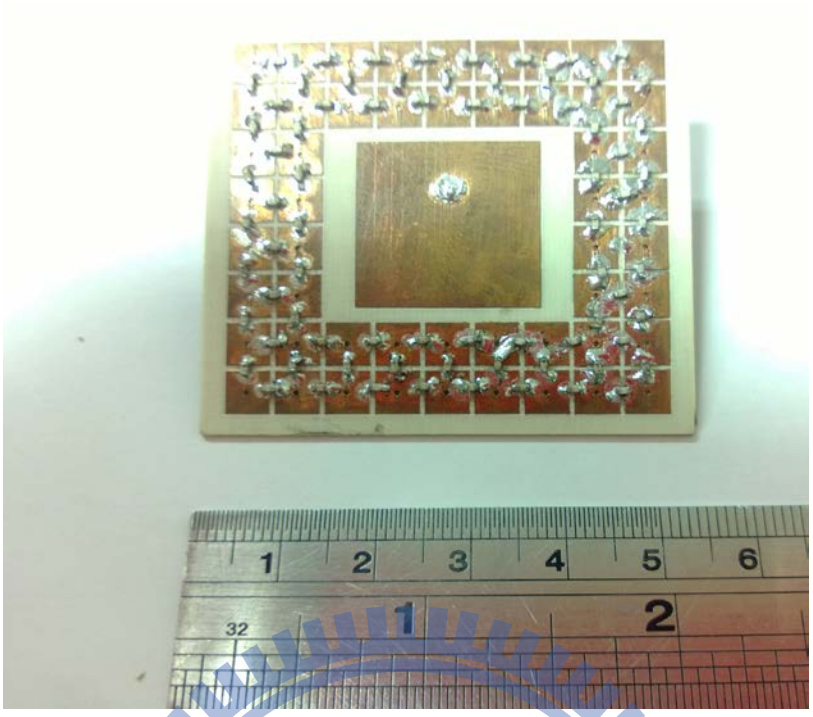

(b)

Figure 5.1(a) Top view of patch anteena and (b) patch antenna with compact mushroom structure

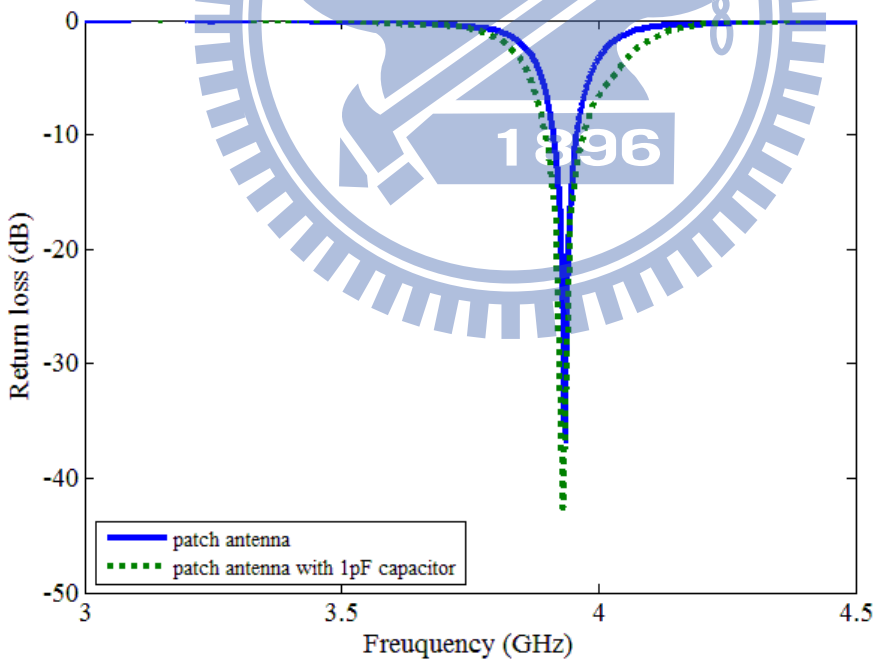

Figure 5.2 return loss of patch antenna and patch antenna with compact mushroom structure

.

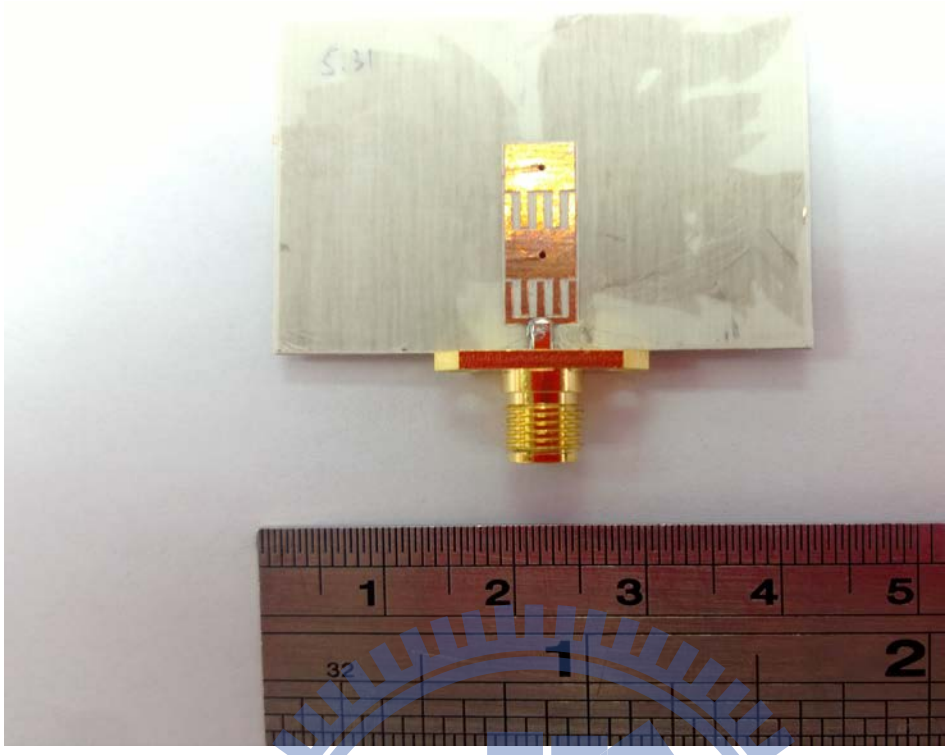

(a)

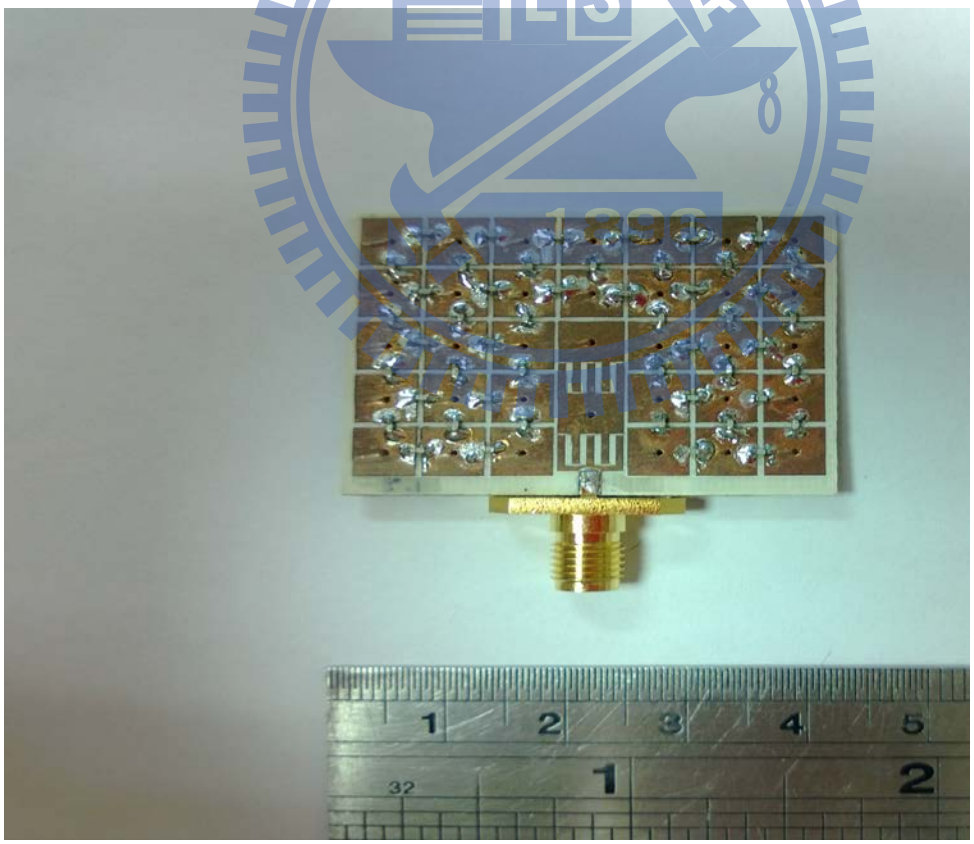

(b)

Figure 5.3(a) CRLH antenna and (b) CRLH antenna with compact mushroom structure

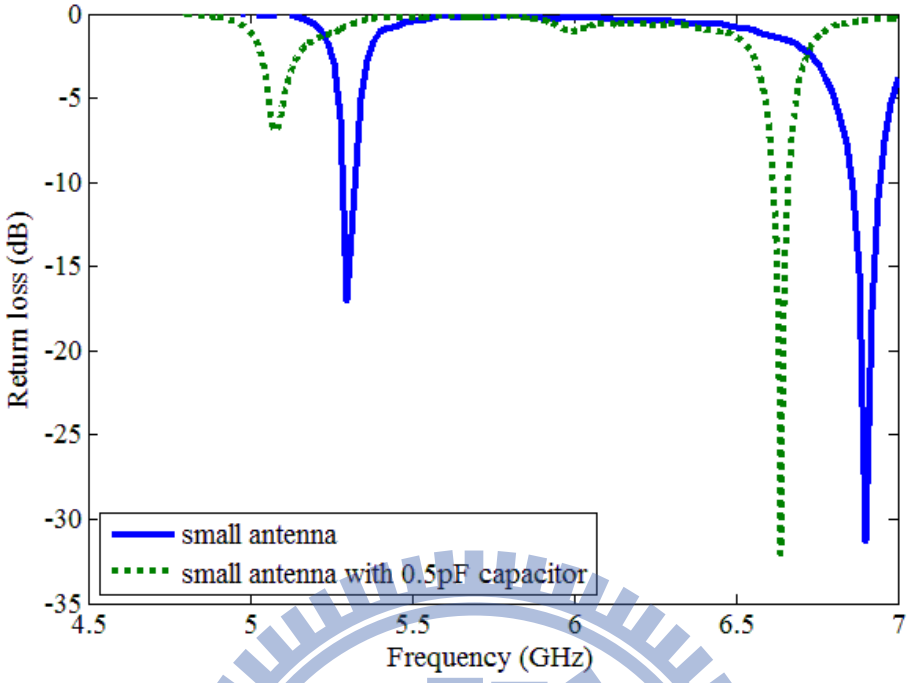

Figure 5.4 Return loss of CRLH antenna and CRLH antenna with compact mushroom structure

Figure 5.1 shows the top view of patch antenna and patch antenna with compact mushroom structure. The measurement results of return loss are shown in Figure 5.2, in which the solid and dotted lines represent the patch antenna and the patch antenna with compact mushroom structure respectively. Both operating frequency are almost the same at 3.9GHz, and it's similar to Figure 4.4. Then the far-field results will be shown in table. 3. Figure 5.3 shows the view of both CRLH antenna and CRLH antenna with compact mushroom structure. The measurement results of return loss are shown in Figure 5.4. Although the operating frequency is shifted to lower frequency which is compared to Figure 4.9, it still have the same trends between simulation results and experiment results. The matching network is affected by compact mushroom structure. In addition, we also measure the efficiency and directivity of both cases, and gain can be converted by efficiency and directivity, as shown in table 3. The efficiency of small antenna by measurement is -5.468dB, and gain is 0.377dB. It seems that the efficiency

is almost as same as total efficiency in table1, but gain is worse. As for the CRLH antenna with the mushroom structure loaded with 0.5pF capacitor, the efficiency is -2.84dB, and the gain is 3.465. It is observed that the efficiency and the gain are improved by accompanying mushroom structure with lumped elements.

Table 3 The measurement results of CRLH antenna and CRLH antenna with mushroom structure

	efficiency	Gain (dB)
patch antenna (3.9GHz)	**72 %**	**5.329**
patch antenna with compact mushroom ctucture (3.9GHz)	**89.15 %**	**6.080**
Small antenna (5.31GHz)	**28.39 %**	**0.377**
Small antenna with compact mushroom (5.1GHz)	**52.00%**	**3.465**

Chapter 6 Conclusion

In chapter 2 and 3, we have seen the effects of mushroom structure by Dispersion diagram simulated by HFSS, and equivalent circuit prediction. And we propose the idea of using lumped element to shift down the bandgap expecting to produce the compact mushroom structure instead of complex design. It can still be analyzed by both methods as mentioned. Considering that we want to observe the bandgap in

practical world, S-parameter measurement can be used to obtain the bandgap effect in insertion loss diagram, including mushroom structure and compact mushroom structure.

In chapter 4, the compact mushroom structure is used for application. We combine both mushroom structure and compact mushroom structure with patch antenna and small antenna. As mentioned before, we know the radiation efficiency has connection with surface wave. We prove that we can use the bandgap effect to improve the performance of antenna by suppressing surface wave affected by mushroom structure and compact mushroom structure. However, the mushroom structure is much larger than small antenna. If the bandgap effect is needed by enough unit cell of mushroom structure to improve performance, ground plane size will be large. Although the antenna is small, the antenna with mushroom structure is large. That can't be call small antenna. So the compact mushroom structure of using lumped element can be used to combine with small antenna to enhance performance but still maintain small size.

REFERENCE

[1] J. Sandra, “Isolation improvement with electromagnetic band gap surfaces.” *Lincoln Laboratory Jour. 19.1 2012.*

[2] D. Sievenpiper, “High-impedance electromagnetic surfaces,” *Ph. D. dissertation, Dept. Elect. Eng., Univ. California at Los Angeles, Los Angeles, CA, 1999.*

[3] D. Bonefa˘ci´c, J. Bartoli´c, “Small antennas: miniaturization techniques and applications.”

[4] F. Yang, and Y. Rahmat-Samii, “Microstrip antennas integrated with electromagnetic band-gap structures: a low mutual coupling design for array applications,” *IEEE Trans. Antennas and Propagat., vol. 51, pp. 2936-2946, Oct 2003*

[5] L.Yang, M.Fan, F. Chen, J. She, and Z. Feng,” A novel compact electromagnetic bandgap structure and its application for microwave circuits,” *IEEE Trans. Mirow. Theory Tech, vol. 53, no 1, pp. 183-190, Jan. 2005.*

[6] E. R. Iglesias, L. I. Sánchez, J. Luis V. Roy, and E. G. Muñoz,” Size reduction of mushroom-type EBG surfaces by using edge-located vias,” *IEEE Microw. wireless Compon lett., vol. 17, no. 9 Sept. 2007.*

[7] S. Clavijo, R. E. Diaz, and W. E. McKinzie III, “ Design methodology for Sievenpiper high-impedance surfaces: an artificial magnetic conductor for positive gain electrically small antennas,” *IEEE Trans. Antennas and Propagat., vol 51, no. 10, Oct. 2003.*

[8] A. Arriola, G. Sasiain, J. I. Sancho, J. Patton, J. Gemio, and R. Villarino, “ Compact high impedance surface based on interdigital capacitors,” *IEEE, Antennas and Propagat., Barcelona, Spain, Apr. 2010*

[9] Y. Fu, N. Yuan, and G. Zhang, “Compact high-impedance surfaces incorporated with interdigital structure,” *IEEE Electronics Lett., vol. 40,no. 5, pp. 310-311, March 2004*

[10] S. Raza, M. A. Antoniades, and V. Eleftheriades, “A compact low-profile high-impedance surface for use as an antenna ground plane,” *IEEE, Antennas and Propagat., Spokane, WA, Jul. 2011.*

[11] K. Ibata, K. Misu, T. Tanagi, H. Oh-hashi, and K. Itoh, “A realistic distributed circuit model for EBG structures based on physical implementations,” *Proc., Chiba, Japan, 2008.*

[12] M. E. Goldfarb, R. A. Pucel, “Modeling via hole grounds in microstrip,” *IEEE Microw. And Guidedw. Lett., vol. 1, no. 6, pp135-137, 1991*

[13] R.Garg, P. Bhartia, and I. Bahl, A. Ittipiboon. “ Microstrip antenna design

handbook," *Boston, London, pp.285-286.*

[14] F. Yang, Y. Rahmat-Samii, " A low-profile circularly polarized curl antenna over an electromagnetic bandgap (EBG) surface," *Microw. Opt. Technol. Lett., vol. 31, no. 4, pp. 264–267, Nov. 2001.*

[15] Y. Zhao, Y. Hao, and C. G. Parini, " Radiation properties of pifa on electromagnetic bandgap structures," *Microw. Opt. Technol. Lett., vol. 44, no. 1, pp. 21–24, 2005.*

[16] M.-J. Lee, S. Pyo, W.-S Shin, and Y.-S Kim, "A size reduced CRLH resonant antenna based on interdigital capacitors with defected ground structure," *Microw. Opt. Tech. Lett., vol. 52, no.9, pp. 2142-2145, Sep. 2010.*